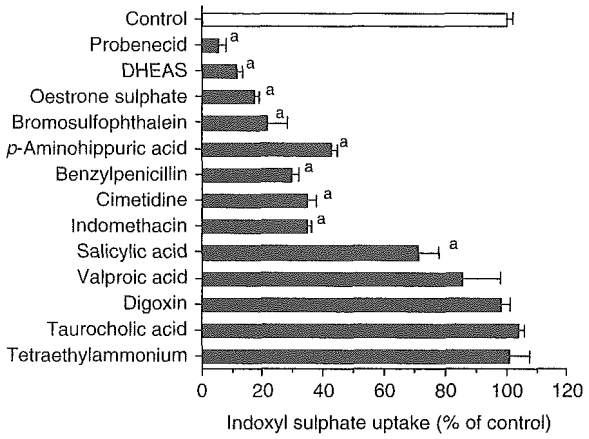

Figure 4. Effect of various compounds on indoxyl sulphate uptake by renal cortical slices. Values are expressed as percentage of indoxyl sulphate uptake by renal cortical slices for 1 h at 25°C in the absence of inhibitors (8.20 ± 0.14 ml/h/g kidney). Concentration of indoxyl sulphate was 20 μM and that of each inhibitor was 400 μM. Each bar represents the mean ± SEM of three different experiments. $^{a}p<0.01$, significantly different from controls

rat kidney indoxyl sulphate is taken up by the same transport system that has a high affinity for oestrone sulphate and DHEAS but only a low affinity for PAH.

Discussion

The disposition of uraemic toxin indoxyl sulphate was characterized in normal and 5/6 nephrectomized (CRF) rats following i.v. administration. The total clearance of indoxyl sulphate was identical to the renal clearance, and it was nearly completely excreted via the kidney (Table 1) in a largely unchanged form. Furthermore, the plasma and renal clearance of indoxyl sulphate was significantly decreased in the CRF rats (Figure 2). These results (Figure 2 and Table 1) indicate that indoxyl sulphate is mainly excreted via the kidney.

Indoxyl sulphate has a high affinity for albumin [3] but is effectively excreted into the urine. Therefore, an active transport system, such as an organic anion transport system, is likely to be involved in its elimination. This assumption is not unreasonable because indoxyl sulphate is an organic acid that contains a sulphate group. Indoxyl sulphate has been reported to inhibit significantly the uptake of PAH in isolated renal tubules [9] and to reduce the renal clearance of PAH [7,8]. Furthermore, our observations indicate that the plasma clearance of indoxyl sulphate is dose-dependent, and both the plasma and renal clearance of indoxyl sulphate was attenuated by the coadministration of PAH and probenecid (Tables 2 and 3). Based on these observations, it is proposed that an organic anion transport system is involved in the active renal secretion of indoxyl sulphate.

To better understand the organic anion transport system and to determine whether it is responsible for the uptake of indoxyl sulphate in the kidney, the mechanism for the uptake of indoxyl sulphate by renal cortical slices was investigated. Renal cortical slices exhibited significant uptake activity for indoxyl sulphate at 25°C (S/M ratio = 8.20 ± 0.14 ml/h/g kidney), whereas under anaerobic conditions at 4°C the extent of uptake was very low (S/M ratio = 1.49 ± 0.18 ml/h/g kidney). The uptake of indoxyl sulphate was found to be a saturable process with a K_m of 43.0 μM, suggesting that an active process is involved in its uptake in the kidney. In the presence of 5% HSA, the K_m for the renal uptake of indoxyl sulphate was 505 μM. The concentration ratio of indoxyl sulphate in the kidney of CRF rats was not different from that in control rats (Figure 1), suggesting that the renal basolateral uptake system responsible for indoxyl sulphate distribution in the tubules was not saturated in the CRF rats. It has been reported that the total serum concentration of indoxyl sulphate is 104–417 μM in chronic renal failure patients [6, 13, 17, 18]. Under this condition, the renal uptake system of indoxyl sulphate would be difficult to saturate. The accumulation of indoxyl sulphate may be related to competitive inhibition by other uraemic toxins such as 3-carboxy-4-methyl-5-propyl-2-furanpropanoic acid (CMPF) and hippuric acid [19, 20].

Furthermore, various anionic compounds inhibited the uptake of indoxyl sulphate in renal cortical slices. These inhibitory effects, particularly by PAH and probenecid, are consistent with the *in vivo* results obtained by integration pharmacokinetics as shown in Table 3. These

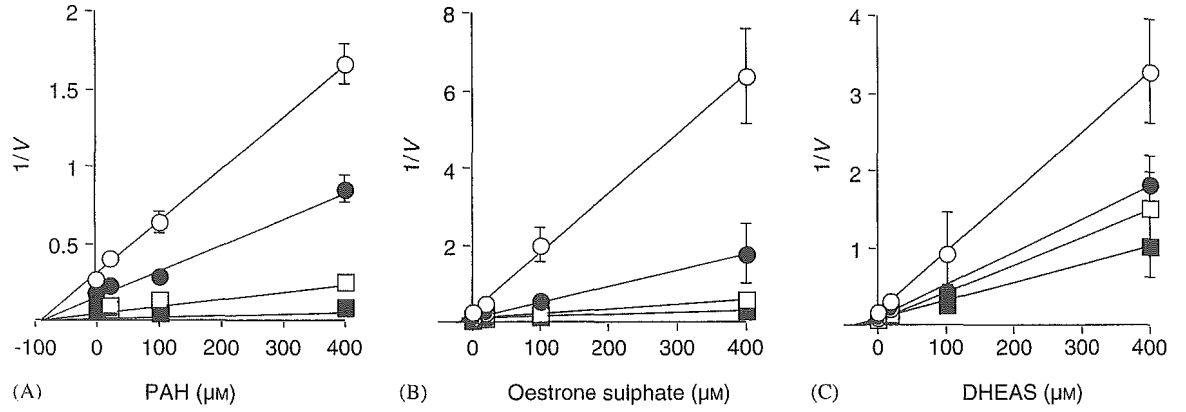

Figure 5. Kinetic analysis of the inhibitory effect of PAH (A), oestrone sulphate (B) and DHEAS (C) on indoxyl sulphate uptake by renal cortical slices. The uptake of indoxyl sulphate (○, 20 μM; ●, 40 μM; □, 120 μM; ■, 240 μM) by renal cortical slices was measured over a 20 min period at 25°C. The K_i value of organic anions for inhibiting indoxyl sulphate uptake was calculated using a Dixon plot. Each bar represents the mean ± SEM of three different experiments

results also support the hypothesis that an organic anion transport system plays an important role in the excretion of indoxyl sulphate in the kidney. The pathway for indoxyl sulphate uptake showed a higher affinity for oestrone sulphate (K_i = 25.1 μM) and dehydroepiandrosterone sulphate (DHEAS) (K_i = 15.8 μM) than for PAH (K_i = 115 μM), which suggests that the indoxyl sulphate transporter has a high affinity for such sulphate conjugates (Figure 5). It has been reported that PAH is a relatively selective substrate for the rat organic anion transporter 1 (rOat1) [21], and that oestrone sulphate has a high affinity for the rat organic anion transporter 3 (rOat3) [22, 23]. Therefore, these results suggest that rOat3 would be important for renal uptake of indoxyl sulphate. It was recently reported that rOat3 could play an important role in the renal uptake of indoxyl sulphate [19]. The present results, including the *in vivo* and *in vitro* studies are consistent with the previous study. In this study, indomethacin showed a significant inhibitory effect for the renal uptake of indoxyl sulphate. This point is not in agreement with our previous study [19]. Considering the evidence that indoxyl sulphate has a relatively low affinity for rOat3 (K_m = 158 μM), the K_m value of the indoxyl sulphate uptake by renal cortical slices (K_m = 43 μM) was lower. These results suggest that other transporters may be involved in this uptake. It has been reported that indoxyl sulphate is a substrate for rOat1 and rOat3 [24], thus a part of the renal uptake of this may involve rOat1. Further investigation will be required to estimate the contribution of these transporters to the renal uptake of indoxyl sulphate.

In uraemia, the accumulation of indoxyl sulphate can lead to the symptoms mentioned above. Indoxyl sulphate may therefore cause other uraemic metabolites and/or drugs to remain in circulation, thus elevating their concentrations to toxic levels. The concentration of indoxyl sulphate was 1.5 times higher in the kidney than in the plasma (Figure 1), thus, indoxyl sulphate may affect the pharmacokinetics of drugs by inhibiting renal excretion. This leads to the suggestion that organic anion transport systems play an important role, not only in the elimination of indoxyl sulphate via the kidney, but also in the mediation of uraemic toxicity by indoxyl sulphate.

Studies have also reported that indoxyl sulphate inhibits thyroxine hepatocyte transport [6] and that the CSF level of indoxyl sulphate is elevated in renal patients with uraemic encephalopathy [1]. The movement of indoxyl sulphate into the brain and liver was lower than into the kidney (Figure 1), whereas the concentration of indoxyl sulphate in the liver (control; 3.13 ± 0.48 nmol/g liver, CRF; 15.2 ± 3.6 nmol/g liver) and the brain (control; 1.11 ± 0.21 nmol/g

brain, CRF; 5.07 ± 1.02 nmol/g brain) was higher than the predicted unbound plasma concentration of indoxyl sulphate (control; 0.22 μmol/l, CRF; 1.35 μmol/l). Furthermore, reports have shown that organic anion transporters such as the OAT family, the oatp family, and the ABC transporter family, exist in other tissues as well as the kidney and function to maintain both cellular and organ homeostasis [25]. Therefore it is likely that a transport system expressed in each individual tissue may mediate uraemic toxicity by transporting indoxyl sulphate [26]. A study of the effects of indoxyl sulphate on such transporters would lead to a better understanding of drug–uraemic toxin interactions, as well as the relationship between uraemic symptoms and uraemic toxins.

In conclusion, the *in vivo* studies showed the highest tissue concentration of indoxyl sulphate in the kidneys, indicative of primary elimination via this organ. This proposal was strongly supported by recovering the major part of injected indoxyl sulphate in urine. Furthermore, using renal cortical slices, it was concluded that the uptake of indoxyl sulphate is mediated by an organic anion transport system.

References

1. Muting D. Studies on the pathogenesis of uraemia. Comparative determinations of glucuronic acid, indican, free and bound phenols in the serum, cerebrospinal fluid, and urine of renal diseases with and without uraemia. *Clin Chim Acta* 1965; **12**: 551–554.
2. Niwa T, Takeda N, Tatematsu A, Maeda K. Accumulation of indoxyl sulphate, an inhibitor of drug-binding, in uraemic serum as demonstrated by internal-surface reversed-phase liquid chromatography. *Clin Chem* 1988; **34**: 2264–2267.
3. Sakai T, Takadate A, Otagiri M. Characterization of binding site of uraemic toxins on human serum albumin. *Biol Pharm Bull* 1995; **18**: 1755–1761.
4. Sakai T, Yamasaki K, Sako T, *et al.* Interaction mechanism between indoxyl sulphate, a typical uraemic toxin bound to site II, and ligands bound to site I of human serum albumin. *Pharm Res* 2001; **18**: 520–524.
5. Tsutsumi Y, Maruyama T, Takadate A, Shimada H, Otagiri M. Decreased bilirubin-binding capacity in uraemic serum caused by an accumulation of furan dicarboxylic acid. *Nephron* 2000; **85**: 60–64.
6. Lim CF, Bernard BF, de Jong M, *et al.* A furan fatty acid and indoxyl sulphate are the putative inhibitors of thyroxine hepatocyte transport in uraemia. *J Clin Endocrinol Metab* 1993; **76**: 318–324.
7. Niwa T, Ise M. Indoxyl sulphate, a circulating uraemic toxin, stimulates the progression of glomerular sclerosis. *J Lab Clin Med* 1994; **124**: 96–104.
8. Niwa T, Ise M, Miyazaki T. Progression of glomerular sclerosis in experimental uraemic rats by administration of indole, a precursor of indoxyl sulphate. *Am J Nephrol* 1994; **14**: 207–212.
9. Boumendil-Podevin EF, Podevin RA, Richet G. Uricosuric agents in uraemic sera. Identification of indoxyl sulphate and hippuric acid. *J Clin Invest* 1975; **55**: 1142–1152.
10. Niwa T. Organic acids and the uraemic syndrome: protein metabolite hypothesis in the progression of chronic renal failure. *Semin Nephrol* 1996; **16**: 167–182.
11. Bueschkens DH, Stiles ME. *Escherichia coli* variants for gas and indole production at elevated incubation temperatures. *Appl Environ Microbiol* 1984; **48**: 601–605.
12. Banoglu E, Jha GG, King RS. Hepatic microsomal metabolism of indole to indoxyl, a precursor of indoxyl sulphate. *Eur J Drug Metab Pharmacokinet* 2001; **26**: 235–240.
13. Sakai T, Maruyama T, Imamura H, Shimada H, Otagiri M. Mechanism of stereoselective serum binding of ketoprofen after hemodialysis. *J Pharmacol Exp Ther* 1996; **278**: 786–792.
14. Tsutsumi Y, Maruyama T, Takadate A, *et al.* Interaction between two dicarboxylate endogenous substances, bilirubin and an uraemic toxin, 3-carboxy-4-methyl-5-propyl-2-furanpropanoic acid, on human serum albumin. *Pharm Res* 1999; **16**: 916–923.
15. Tsutsumi Y, Deguchi T, Takano M, *et al.* Renal disposition of a furan dicarboxylic acid and other uraemic toxins in the rat. *J Pharmacol Exp Ther* 2002; **303**: 880–887.
16. Yamaoka K, Tanigawara Y, Nakagawa T, Uno T. A pharmacokinetic analysis program (multi) for microcomputer. *J Pharmacobiodyn* 1981; **4**: 879–885.
17. Stanfel LA, Gulyassy PF, Jarrard EA. Determination of indoxyl sulphate in plasma of patients with renal failure by use of ion-pairing liquid chromatography. *Clin Chem* 1986; **32**: 938–942.
18. Niwa T, Miyazaki T, Tsukushi S, *et al.* Accumulation of indoxyl-beta-D-glucuronide in uraemic serum: suppression of its production by oral sorbent and efficient removal by hemodialysis. *Nephron* 1996; **74**: 72–78.
19. Deguchi T, Ohtsuki S, Otagiri M, *et al.* Major role of organic anion transporter 3 in the transport of indoxyl sulphate in the kidney. *Kidney Int* 2002; **61**: 1760–1768.
20. Motojima M, Hosokawa A, Yamato H, Muraki T, Yoshioka T. Uraemic toxins induce proximal tubular injury via organic anion transporter 1-mediated uptake. *Br J Pharmacol* 2002; **135**: 555–563.
21. Hasegawa M, Kusuhara H, Sugiyama D, *et al.* Functional involvement of rat organic anion transporter 3 (rOat3; Slc22a8) in the renal uptake of organic anions. *J Pharmacol Exp Ther* 2002; **300**: 746–753.
22. Nagata Y, Kusuhara H, Endou H, Sugiyama Y. Expression and functional characterization of rat organic anion

transporter 3 (rOat3) in the choroid plexus. *Mol Pharmacol* 2002; **61**: 982–988.
23. Kusuhara H, Sekine T, Utsunomiya-Tate N, *et al*. Molecular cloning and characterization of a new multispecific organic anion transporter from rat brain. *J Biol Chem* 1999; **274**: 13675–13680.
24. Enomoto A, Takeda M, Tojo A, *et al*. Role of organic anion transporters in the tubular transport of indoxyl sulphate and the induction of its nephrotoxicity. *J Am Soc Nephrol* 2002; **13**: 1711–1720.
25. Kusuhara H, Sugiyama Y. Role of transporters in the tissue-selective distribution and elimination of drugs: transporters in the liver, small intestine, brain and kidney. *J Control Release* 2002; **78**: 43–54.
26. Ohtsuki S, Asaba H, Takanaga H, *et al*. Role of blood–brain barrier organic anion transporter 3 (OAT3) in the efflux of indoxyl sulphate, a uraemic toxin: its involvement in neurotransmitter metabolite clearance from the brain. *J Neurochem* 2002; **83**: 57–66.

Available online at www.sciencedirect.com
SCIENCE DIRECT®
Biochimica et Biophysica Acta 1623 (2003) 88–97
BIOCHIMICA ET BIOPHYSICA ACTA
BBA
www.bba-direct.com

The effect of glycation on the structure, function and biological fate of human serum albumin as revealed by recombinant mutants

Keisuke Nakajou[a], Hiroshi Watanabe[a], Ulrich Kragh-Hansen[b], Toru Maruyama[a], Masaki Otagiri[a,*]

[a] *Department of Biopharmaceutics, Graduate School of Pharmaceutical Sciences, Kumamoto University, 5-1 Oe-honmachi, Kumamoto 862-0973, Japan*
[b] *Department of Medical Biochemistry, University of Aarhus, DK-8000 Århus, Denmark*

Received 12 June 2003; received in revised form 29 July 2003; accepted 7 August 2003

Abstract

Recombinant wild-type human serum albumin (rHSA), the single-residue mutants K199A, K439A and K525A and the triple-residue mutant K199A/K439A/K525A were produced using a yeast expression system. Portions of the rHSA were glycated to different degrees (2.5–250 mM D-glucose). As detected by far-UV and near-UV CD, intrinsic tryptophan-fluorescence and probed by 1,1′-bis(4-anilino)naphthalene-5,5-disulfonic acid, the single-residue mutations had no effect on albumin conformation, whereas the triple-residue mutation and glycation caused conformational changes. The triple-residue mutation and glycation had comparable increased effects on high-affinity binding of warfarin (site I), but decreased effects on high-affinity binding of dansylsarcosine (site II) and the esterase-like activity of albumin. The relation between plasma half-lives in rats were found to be glycated rHSA (50 mM glucose) < triple-residue mutated rHSA < rHSA. The opposite trend was found for liver and kidney uptakes in mice. Even though the functional and the in vivo properties of rHSA could be effected differently by the minor conformational changes caused by the triple-residue mutation and glycation, the present findings indicate that the effect of glycation can be partly explained by blockage of the positive charges of lysine at positions 199, 439 and 525.

Keywords: Human serum albumin; Glycation; Positive charge; Organ uptake; Site-directed mutagenesis

1. Introduction

Human serum albumin (HSA) is a single-chain protein synthesized in and secreted from liver cells. Normally, it is a simple protein, i.e. it is without prosthetic groups and covalently bound carbohydrate or lipid [1]. Based on X-ray crystallographic analyses of HSA and its recombinant version (rHSA), the polypeptide chain of 585 amino acids forms a heart-shaped protein with dimensions 80 × 80 × 80 Å and with a thickness of 30 Å [2,3]. The protein has three homologous domains (I–III), and each of these is comprised of two subdomains (A and B).

In the circulation, HSA becomes nonenzymatically glycated by reducing sugars, and the reference range in normal humans is 6–10% glycoalbumin. However, this proportion typically increases to between 20% and 30% in hyperglycemic patients [4]. As a result, glycoalbumin has been proposed as a useful test for short-term control (2–4 weeks) of diabetics [1]. By contrast, glycohemoglobin (hemoglobin A_{IC}) is the favorite test for monitoring long-term control of blood sugar levels in diabetics.

Functional studies have been performed with HSA glycated with D-glucose, but disagreement seems to exist on whether or not glycation affects, e.g. the unique ligand binding properties of the molecule. Thus, reports of increased, decreased and unmodified ligand binding have appeared [1,5]. In cases of effects on binding, the issue of whether the effect is caused by the presence as such of the covalently bound glucose, blockage of charged residue(s) of the protein or a combination of both mechanisms has not been evaluated. Furthermore, the possible effect of glycation on the structure of HSA has not been studied much.

The principal site of glycation of HSA is Lys-525, but the lysine residues in positions 199, 281 and 439 are also

Abbreviations: HSA, human serum albumin isolated from serum; rHSA, recombinant human serum albumin; bis-ANS, 1,1′-bis(4-anilino)naphthalene-5,5-disulfonic acid

* Corresponding author. Tel.: +81-96-371-4150; fax: +81-96-362-7690.
E-mail address: otagirim@gpo.kumamoto-u.ac.jp (M. Otagiri).

0304-4165/$ - see front matter © 2003 Elsevier B.V. All rights reserved.
doi:10.1016/j.bbagen.2003.08.001

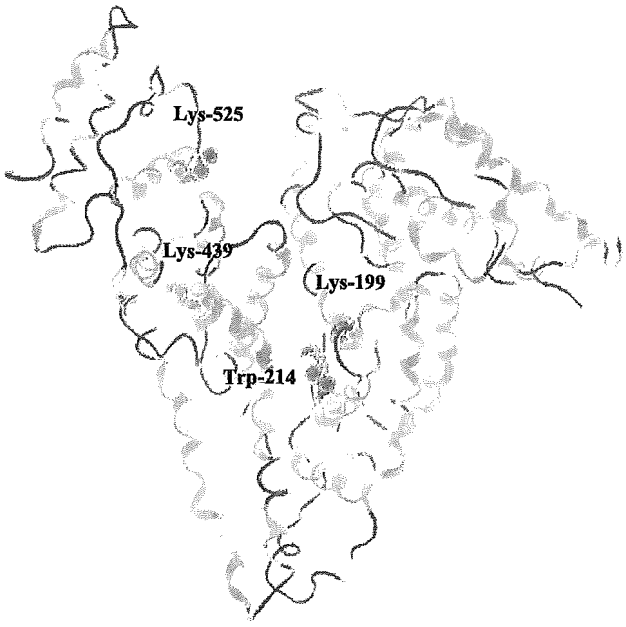

Fig. 1. Location of mutation sites and Trp-214 in rHSA.

susceptible to glycation. In addition, six other residues of less importance have been identified [6–8]. In an attempt to shed some light on the above aspects, we produced nonglycated and glycated wild-type rHSA, the single-residue mutants K199A, K439A, K525A and a triple-residue mutant in which all three lysine residues had been substituted with alanine (Fig. 1). For the production of recombinant albumin, we used an expression strain of the methylotrophic yeast *Pichia pastoris*. Attempts to produce K281A failed due to its lack of excretion. The possible effect of mutation or glycation on protein structure was examined by a variety of spectroscopic approaches, and any effects on ligand binding were examined using the test-ligands warfarin and dansylsarcosine, which bind to two important ligand binding regions of HSA (site I and site II, respectively [1]). The effects of mutation and glycation on the esterase-like activity of rHSA was also examined. Finally, we investigated the pharmacokinetics of mutated and glycated rHSA using the ^{125}I-labeled protein in rats and ^{111}In-labeled protein in mice. In all experiments, nonglycated rHSA was used as a control because it is certain that this albumin preparation, in contrast to HSA, is devoid of carbohydrate.

2. Materials and methods

2.1. Materials

Restriction enzymes, T4 polynucleotide kinase, calf intestinal alkaline phosphatase, a DNA ligation kit and TaKaRa EX Taq DNA polymerase were obtained from Takara Shuzo Co. Ltd. (Kyoto, Japan). A DNA sequence kit was obtained from Perkin-Elmer Applied Biosystems (Tokyo, Japan). The *Pichia* Expression kit was purchased from Invitrogen Co. (San Diego, CA, USA).

HSA was donated by the Chemo-Sera-Therapeutic Research Institute (Kumamoto, Japan) and was defatted by treatment with charcoal as described by Chen [9]. Blue Sepharose CL-6B was purchased from Amersham Pharmacia Biotech (Uppsala, Sweden). 1,1′ -bis(4-anilino)naphthalene-5,5-disulfonic acid (bis-ANS) and dansylsarcosine were from Sigma Chemical Co. (St. Louis, MO, USA). Potassium warfarin was donated by Eisai Co. (Tokyo, Japan). *p*-nitrophenyl acetate was obtained from Nakalai Tesque (Kyoto, Japan). D(+)-Glucose (in excess of 98.0% purity) was from Wako Pure Chemical Industries, Ltd. (Osaka, Japan). Na^{125}I (17.4 Ci/mg in pH 10-NaOH) was bought from NEN (Boston, MA, USA). $^{111}InCl_3$ (74 Mbq/ml in 0.02 N HCl) was a gift from Nihon Medi-Physics (Takarazuka, Japan). Other chemicals were also of the best grades commercially available.

2.2. Synthesis and purification of rHSA forms

The recombinant DNA techniques used in producing wild-type rHSA, three single-residue mutants and a triple-residue mutant have essentially been described previously [10]. A chimaeric plasmid (pJDB-ADH-L10-HSA-A) having cDNA for the mature form of HSA along with an L10 leader sequence was a gift from the Tonen Co. (Tokyo, Japan). The mutagenic primers used (underlined letters indicate mismatches) were: 5′-CAAACAGAGACT CGCC TGTGCCAGTCTCC-3′ for K199A; 5′-GCAAATGTTGTGCA CATCCTGAAGC-3′ for K439A; and 5′-GACAAATCAAGGCA CAAACTGCAC-3′ for K525A. For preparing the triple-residue mutant, all three mutagenic primers were used. The L10-HSA coding region was amplified by PCR with a forward and a reverse primer carrying a 5′-terminal *Eco*RI site and cloned into the *Eco*RI-digested pKF19k vector (Takara Shuzo). Mutagenesis was carried out using a site-directed mutagenesis kit (oligonucleotide-directed dual amber method) obtained from Takara Shuzo. The mutation was confirmed by DNA sequencing of the entire HSA coding region using the dideoxy chain termination method with a Perkin-Elmer ABI Prism 310 Genetic Analyzer. For constructing the HSA expression vector pHIL-D2-HSA, an L10-HSA coding region without or with the desired mutation site(s) was incorporated into the methanol inducible pHIL-D2 vector (Invitrogen). The resulting vector was introduced into the yeast species *P. pastoris* (strain GS115) for rHSA expression. Secreted rHSA was isolated from the growth medium by a combination of precipitation with 60% (w/v) ammonium sulfate and purification on a Blue Sepharose CL-6B column. Isolated protein was defatted using the charcoal procedure, as described by Chen [9], deionized, freeze-dried and then stored at −20 °C until used. The resulting albumins (treated with dithiothreitol) exhibited a single band on SDS/PAGE gel, and

all the recombinant proteins migrated at the same position as HSA (results not shown). Density analysis of Coomassie Brilliant Blue-stained protein bands showed that the purity of the recombinant albumins was in excess of 97%.

2.3. Glycation of wild-type rHSA

A solution of rHSA (5 mg/ml) with glucose (2.5, 12.5, 50 or 250 mM) was prepared in 67 mM sodium phosphate buffer, pH 7.4. After sterilization by filtration (0.22 μm filters, Millipore), the solutions were incubated at 37 °C for 60 days in the absence or presence of 20 μM copper sulfate [4,11]. After incubation, reversibly bound and unbound glucose were removed by extensive dialysis against H_2O. The proteins were then freeze-dried and stored at −20 °C. As a control, rHSA alone was treated in the same manner. The percentage of rHSA glycated with 50 mM glucose was determined by an affinity chromatographic method using a boronic acid-agarose column [12] and was found to be 71% (bound to boronate column). The number of modified lysine residues was about 8.9 residues per mole of rHSA at 50 mM glucose [13]. The formation/presence of cross-links (dimers or oligomers) and fragmentation were negligible when checked by SDS/PAGE. Moreover, structural differences between the samples prepared with or without copper sulfate were not observed, as will be described later. The protein concentration in this and the following types of experiments were obtained by dissolving a known amount of freeze-dried powder in a desired volume of buffer.

2.4. Spectroscopic studies

2.4.1. Intrinsic CD spectra

CD measurements were made with a Jasco J-720 type spectropolarimeter (Tokyo, Japan). Far-UV intrinsic spectra were recorded from 200 to 250 nm using a protein concentration of 1.5 μM in 67 mM sodium phosphate buffer (pH 7.4, 25 °C). Near-UV spectra were obtained from 250 to 350 nm at a protein concentration of 15 μM in the same buffer. For calculation of the mean residue ellipticity, [θ], the molecular masses of the albumins were assumed to be 66.5 kDa.

2.4.2. Intrinsic fluorescence measurements

Intrinsic fluorescence spectra were obtained with a Jasco FP-770 fluorimeter (Tokyo, Japan). The albumins were excited at 295 nm, and the spectra were corrected for buffer baseline fluorescence. The protein concentrations were 15 μM in 67 mM sodium phosphate buffer at pH 7.4 and 25 °C.

2.4.3. Effective hydrophobicity

The effective hydrophobicity of albumin (1 μM), as dissolved in the phosphate buffer, was probed with bis-ANS (10 μM) at 25 °C. The compound was excited at 394 nm, and fluorescence spectra were obtained with the Jasco FP-770 fluorimeter.

2.5. Ligand binding experiments

2.5.1. Fluorescence measurements

Fluorescence measurements were made on the Jasco FP-770 fluorimeter. The fluorophores of warfarin and dansylsarcosine were excited at 320 and 350 nm, respectively. The fluorescence emission intensities were measured at maximum wavelengths (approx. 380 nm for warfarin and approx. 480 nm for dansylsarcosine). When these molecules bind to albumin, the intensities of their fluorescence emissions are enhanced approximately 10-fold over that observed for their unbound states. To calculate the binding constants for the warfarin–protein and dansylsarcosine–protein interactions, three separate titrations were performed according to a previously outlined procedure [14,15], and the data were evaluated according to Maes et al. [16]. For estimating the molar fluorescence of 100% protein-bound ligand, only data points at a ligand–protein molar ratio higher than 1:10 were used in order to keep the error of the extrapolation under 1%, as described by Rajkowski [17]. All fluorescence intensities were corrected for inner filter effects and for buffer baseline fluorescence.

2.5.2. Binding data analysis

Binding constants were estimated by fitting the experimental data to the following general equation using a non-linear least-squares computer program (MULTI program):

$$r = \frac{[L_b]}{[P_t]} = \Sigma \frac{n_i K_i [L_f]}{1 + K_i [L_f]}$$

In this equation, r denotes the number of moles of ligand bound per mole of protein, $[L_b]$ and $[L_f]$ the bound and unbound ligand concentrations, respectively, and $[P_t]$ the protein concentration. K_i and n_i are the association constant and the number of binding sites for the ith class of binding sites, respectively. At the molar ratios between ligand and albumin (≤ 0.4) used in this study, the binding results could be well-characterized by assuming binding to only the high-affinity binding site. Therefore, only K_1-values were calculated.

2.6. Determination of esterase-like activity

The reaction of *p*-nitrophenyl acetate with albumin was followed spectrophotometrically at 400 nm (Jasco Ubest-35 UV/VIS spectrophotometer) by monitoring the appearance of *p*-nitrophenol. The reaction mixtures contained 5 μM *p*-nitrophenyl acetate and 20 μM albumin in 67 mM sodium phosphate buffer (pH 7.4). Reactions were followed at 25 °C. Under these conditions pseudo-first-order rate constant analysis could be applied, as described

in previous reports [18,19], and hydrolysis rate constants (k_{obs}) were calculated.

2.7. In vivo studies

2.7.1. ^{125}I labeling

The chloramine-T method was used to label the rHSA forms with ^{125}I [20]. Eighty-five microliters of 0.4 M sodium phosphate buffer (pH 7.5) and 10 μl $Na^{125}I$ were added to 5 μl of protein solution (1 mg/ml) and mixed on ice. Ten microliters of chloramine-T diluted in ice-cold distilled water to 3.8 mM was added, and the resulting solution was mixed for 30 s; this procedure was performed three times. Finally, 100 μl of sodium metabisulfite solution (2.5 mM) was added and mixed for 30 s. For removing unreacted ^{125}I, the solution was applied to a PD-10 column (Pharmacia) and eluted with phosphate buffer (0.25 M, pH 7.5) containing 0.2% bovine serum albumin. The eluents were collected in plastic tubes, and the radioactivity was counted using a well counter (ARC 2000, Aloka, Tokyo, Japan). Appropriate fractions were collected, pooled and stored at −80 °C until used. The specific activity of the samples was about 200×10^6 cpm/μg protein.

2.7.2. Rat experiments

Male Wistar rats (230 g) maintained on a standard rat food and water diet were anaesthetized with diethylether. ^{125}I-labeled protein was injected into the vena cava superior at a dose of 0.01 mg/kg. Blood was collected after 3 min and after 1, 2, 4, 8, 24 and 48 h of injection. Blood samples were centrifuged at 3000 rpm for 10 min after which, 20 μl of the plasmas formed were diluted by adding 80 μl of a 5% HSA solution followed by the addition of 100 μl of 25% trichloroacetic acid (TCA). After 1 h on ice, the samples were centrifuged at 3000 rpm for 10 min. The supernatants were removed and 200 μl of 12.5% TCA was added to the precipitate. After mixing, the solutions were centrifuged at 3000 rpm for 10 min. The supernatants were separated, and the radioactivity of the TCA-precipitable fractions were determined.

2.7.3. ^{111}In labeling

^{111}In labeling of albumins was performed using diethylenetriaminepentaacetic acid (DTPA) as the bifunctional chelating agent as described by Hnatowich et al. [21]. DTPA was attached to albumin by dissolving the protein (5 mg) in 1 ml of 4-(2-hydroxyethyl)-1-piperazineethane sulfonic acid buffer (0.1 M, pH 7.0), and then adding a 2-fold molar excess of DTPA anhydride in 10 μl of dimethyl sulfoxide. After stirring for 1 h at room temperature, unreacted DTPA was removed by placing the solution on a Sephadex G-25 column (1 × 40 cm) followed by elution with acetate buffer (0.1 M, pH 6.0). Fractions containing DTPA-albumin were selected using spectrophotometry (280 nm) and concentrated by an ultrafiltration apparatus from Advantec (Dublin, CA, USA).

Twenty microliters of $^{111}InCl_3$ solution, 60 μl of DTPA-albumin and 20 μl of sodium acetate buffer (1 M, pH 6.0) were mixed. After standing for 30 min at room temperature, unreacted $^{111}InCl_3$ was removed by adding the solution to a PD-10 column followed by elution with acetate buffer (0.1 M, pH 6.0). The ^{111}In-enriched fractions were selected on the basis of their radioactivity and concentrated by ultrafiltration. Radioactivity was determined with a well counter. The specific activity of the pooled samples was about 3×10^4 cpm/μg protein. In this case, the protein concentration was determined using the Bradford assay.

2.7.4. Mice experiments

Prior to administration, trace amounts of radiolabeled proteins were diluted with saline, and the protein concentration was adjusted to 0.1 mg/ml by adding nonlabeled protein. Radiolabeled and nonlabeled proteins (0.1 mg/kg, 10 kcpm) were injected as a bolus into the tail vein of mice anaesthetized with diethylether [21,22]. After 1, 3, 5, 10 or 30 min, the animals were killed by bleeding and the liver and the kidneys were excised. Samples of liver and kidney were used for counting.

2.7.5. Data analysis

The radioactivity of liver and kidney samples was used to calculate the apparent uptake clearances of albumin [22,23]. The radioactivity of all samples was related (percentages) to the total dose given to the animals. In order to calculate uptake clearances, the relative radioactivities were analyzed by a biexponential function using the non-linear least-squares computer program MULTI.

Assuming zero or negligible leakage of radioactivity from organs, the apparent organ uptake clearance (CL_{organ}) may be expressed as:

$$CL_{organ} = \frac{X_{t_i}}{AUC_{t_0-t_i}}$$

where X_{t_i} is the amount of radioactivity in the organ of interest at the end of the 30 min experiment, and $AUC_{t_0-t_i}$ the area under the curve for the time interval from $t_0 = 0$ min to $t_i = 30$ min.

3. Results and discussion

3.1. Structural properties

The structural properties of rHSA and glycated rHSA were examined by far-UV and near-UV CD spectroscopy (Fig. 2). The far-UV (Fig. 2A) and near-UV CD spectra (Fig. 2B) of rHSA treated with low glucose concentrations, 2.5 or 12.5 mM glucose, are nearly identical with those of rHSA. However, for rHSA glycated with 50 or, especially, 250 mM glucose, changes in the secondary structures were

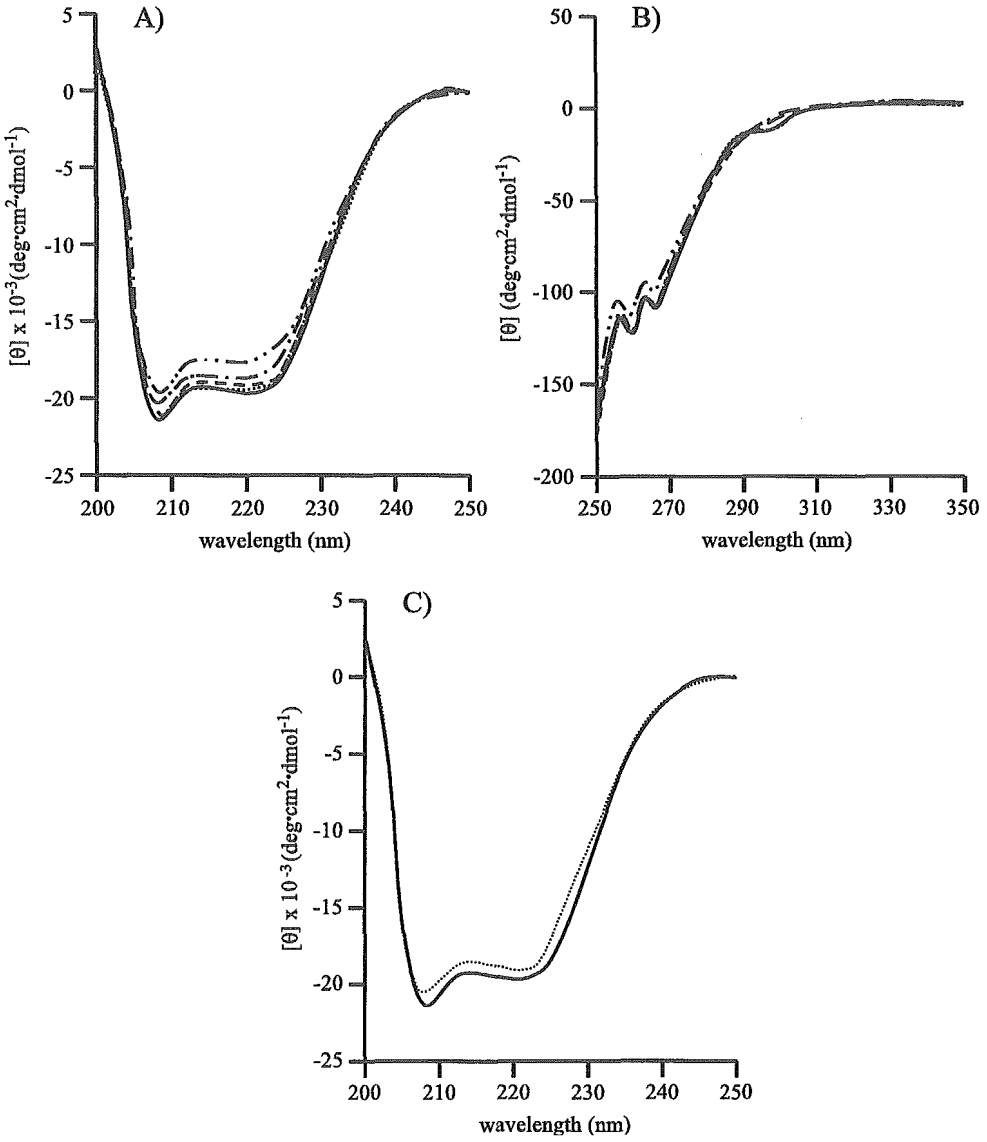

Fig. 2. Far-UV and near-UV CD spectra of rHSA forms at 25 °C. The protein concentration was 1.5 μM (A and C) or 15 μM (B) in 67 mM sodium phosphate buffer (pH 7.4). (A) Far-UV CD spectra and (B) near-UV CD spectra of rHSA and glycated rHSAs. Spectra are shown for rHSA (—) and rHSA glycated with 2.5 (. . . . .), 12.5 (- - -), 50 (—·—·—) or 250 (—··—·) mM glucose. (C) Far-UV CD spectra of rHSA (—) and triple-residue mutant (. . . . .). Sterile incubation for 60 days at 37 °C had no appreciable effect on the spectra for rHSA. The spectra are averages of three experiments.

observed. In the following experiments, rHSA treated with 50 mM glucose was mainly studied because this preparation clearly showed the effects of glycation, and because the glucose concentration is not unrealistically high.

The effect of mutation was also examined by CD-spectroscopy. As can be seen from Fig. 2C, triple-residue mutation caused conformational changes. In the case of the single-residue mutants, no spectral changes were detected, compared with the spectrum of rHSA (results not shown). The near-UV CD spectra were not affected to any extent by the different protein mutations (results not shown).

HSA has a single tryptophanyl residue at position 214. In order to obtain detailed information concerning the environment of this residue, tryptophan emission spectra were obtained after excitation at 295 nm. Fig. 3 shows that the relative fluorescence intensities at λ_{max} for the triple-residue mutant and the glycated protein are reduced to 67% and 51%, respectively. In addition, λ_{max} was slightly blue-shifted, namely from 345 to 341 nm for the mutant and to 343 nm in case of glycated rHSA. In contrast, the spectra obtained for the single-residue mutants were very similar to that of rHSA (results not shown). We suggest that the changes of tryptophan fluorescence observed for the triple-residue mutant and the glycated protein could result from various causes such as changed location of the tryptophan ring, possible interaction with other amino acid residue or overall protein structure changes. In contrast, it is unlikely that the decrease in fluorescence of the glycated

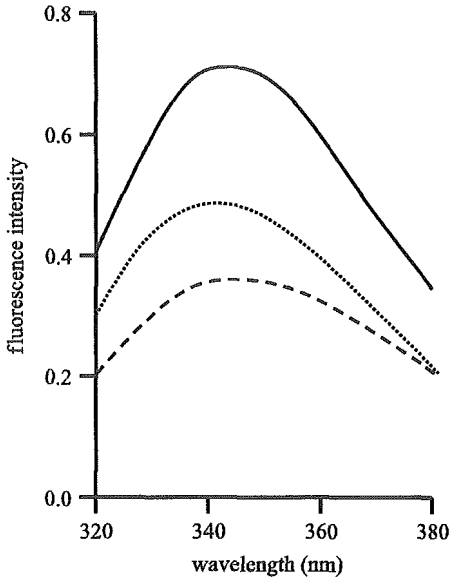

Fig. 3. Intrinsic fluorescence spectra of rHSA forms at 25 °C. The proteins were excited at 295 nm at a concentration of 15 μM in 67 mM sodium phosphate buffer (pH 7.4). Spectra are shown for rHSA (—), the triple-residue mutant (. . . . . .), and for rHSA glycated with 50 mM glucose (- - -). Sterile incubation for 60 days at 37 °C had no appreciable effect on the spectrum for rHSA. The spectra are averages of three experiments.

protein is caused by the direct binding of glucose to Trp-214, because among the 10 residues known to be involved in glycation, tryptophan is not included [6–8].

On the other hand, the glycation of proteins is generally accompanied by oxidation. Elevated levels of metal ions such as iron and copper have been reported for diabetic patients. In addition, free radicals have been shown to be generated by the presence of glycated proteins, which in turn accelerate the glycation reaction [24]. In this study, "glycoxidation" products might have been produced by incubation of rHSA and glucose in the presence of copper ions. However, no differences in the fluorescence and CD spectra as well as SDS/PAGE of samples prepared with and without copper ions were observed under the present experimental conditions. Thus, it is not likely that the reduced fluorescence described above is due to oxidation of the tryptophan residue itself [25].

The effect of triple-residue mutation and glycation on the degree of exposure of hydrophobic areas was evaluated using the fluorescent probe bis-ANS [26,27]. The fluorescence of bis-ANS is enhanced on binding to the albumins. As can be seen from the fluorescent data in Fig. 4, the relative fluorescence intensities at λ_{max} for the mutated and glycated protein is reduced to 73% and 63%, respectively. Furthermore, the λ_{max} of bis-ANS bound to the mutant and the glycated rHSA were blue-shifted from 500 nm for rHSA to 496 and to 495 nm, respectively. The reduced fluorescence intensities for the mutant and the glycated rHSA are most probably due to weaker binding, compared with the binding to rHSA. In contrast, the spectra for the single-residue mutants were not significantly affected (results not shown).

Thus, simultaneous mutation of lysine in positions 199, 439 and 525, but not of the individual residues, as well as glycation results in slight conformational changes in rHSA. These involve the secondary structure and the effective hydrophobicity of the protein and most likely involves the vicinity of Trp-214.

3.2. Functional properties

3.2.1. Ligand binding

The unique ligand binding properties of HSA can, to a great extent, be explained by the presence of two major binding regions, site I and site II, which are located within specialized cavities in subdomain IIA and IIIA, respectively [1]. Since the effect of glycation on ligand binding seems to be unclear, we examined the binding of warfarin and dansylsarcosine, which bind with high affinity to site I and site II, respectively. In these and the following experiments, our attention was focused on rHSA, the triple-residue mutant and glycated rHSA. The binding constant for the interaction of warfarin with rHSA was estimated to be $4.38 \times 10^5\ M^{-1}$ (Table 1), which is in reasonable agreement with that previously obtained at this laboratory [14].

The table also shows that both mutating and glycating albumin increased warfarin binding; the association constant was increased by a factor 1.6–1.8. The effect of a mutated

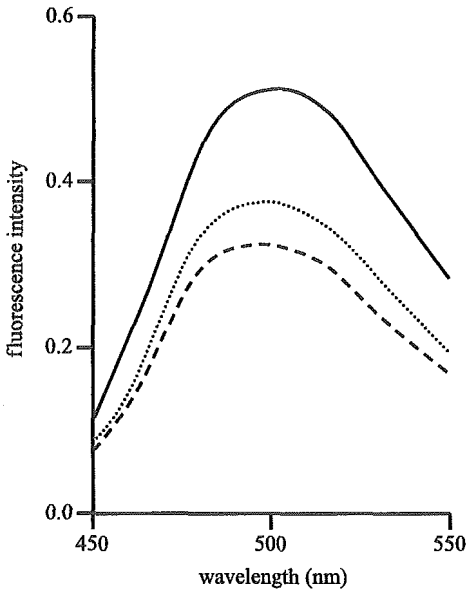

Fig. 4. Evaluation of effective hydrophobicity of rHSA forms at 25 °C using bis-ANS. The fluorophore was excited at 394 nm, and the concentrations of bis-ANS and protein was 10 and 1 μM, respectively. The medium was 67 mM sodium phosphate buffer (pH 7.4). Spectra are shown for rHSA (—), the triple-residue mutant (. . . . . .), and for rHSA glycated with 50 mM glucose (- - -). Sterile incubation of rHSA for 60 days at 37 °C had no appreciable effect on the spectrum for bis-ANS. The spectra are averages of three experiments.

Table 1
High-affinity binding of warfarin and dansylsarcosine to rHSA forms at pH 7.4 and 25 °C

rHSA	Association constant (10^5 M^{-1})	
	Warfarin (site I)	Dansylsarcosine (site II)
Wild-type	4.38 ± 0.11	12.99 ± 0.33
Triple-residue mutant	7.34 ± 0.40	2.59 ± 0.47
Glycated wild-type (2.5 mM)	6.84 ± 0.39	9.43 ± 0.31
(12.5 mM)	7.76 ± 0.28	6.58 ± 0.17
(50 mM)	7.89 ± 0.20	3.27 ± 0.54

The albumin concentration was 10 μM, whereas the total concentration of both ligands varied from 0.5 to 4 μM. The experiments were performed in 67 mM sodium phosphate buffer. The values given are the means ± S.D. of three experiments.

Lys-199, which is in site I (at the pocket entrance), on warfarin binding is most probably a direct one [14]. Recently, Petersen et al. [28] showed that the single mutation K199M had an increased affinity for warfarin by a factor of two. It thus seems possible that the effects on warfarin binding found in this work may be entirely attributable to the K199A substitution. In contrast to warfarin binding, the binding of the site II-marker ligand dansylsarcosine was decreased by the protein manipulations. Thus, the binding constant was decreased about five times for mutated rHSA. Furthermore, for rHSA treated with 50 mM glucose the constant was decreased about four times. The diminished binding properties for dansylsarcosine reflect conformational changes involving site II. It is also possible that arginine modification by dicarbonyls such as glyoxal and methylglyoxal, which are produced by glucose autoxidation and have high reactivity with arginine residues, can cause or contribute to the decreased dansylsarcosine binding [29,30]. However, the effect of arginine modification on the binding may be small, considering from our previous findings that the single mutation R410A lost significantly its ligand binding ability [31].

In agreement with the present results, Okabe and Hashizume [32] found that the induced ellipticity of HSA caused by warfarin binding was enhanced by glycation. The same authors reported a pronounced diminishing effect of glycation on the binding of the site II-ligands dansylproline and ibuprofen. However, they also reported an enhancement in the binding of relatively low concentrations of flufenamic acid, another site II-ligand. Bohney and Feldhoff [33] observed no effect of glycation on L-tryptophan binding to site II. Any discrepancies between the present study and those just cited, are probably due to differences in type of ligand and/or incubation conditions.

3.2.2. Esterase-like activity

In addition to ligand binding, HSA has several other functions, including esterase-like activity which is largely due to the close proximity of Arg-410 and Tyr-411 in site II [31]. The effect of mutation or glycation on that property of albumin was studied using *p*-nitrophenyl acetate as a substrate. As seen in Table 2, the k_{obs} values decreased by glycation. The triple-residue mutant and rHSA treated with 50 mM glucose had similar esterase-like activities, because the activities were decreased to 40% and 41% of the original level in case of mutation and glycation, respectively. The diminished activities are likely to be caused by conformational changes which increase the distance between the active groups of Arg-410 and Tyr-411. The glycated rHSA has not been well characterized in this study. However, the extent of glycated Arg-410 may be small because the modification of Arg-410 residue may significantly affect the esterase activity as well as the ligand binding, as mentioned above [31]. Therefore, the effect of glycation could also partly be due to modification of Arg-410 by dicarbonyls. Thus, triple-mutation and glycation have diverse effects on different parts of the albumin molecule. Warfarin binding to site I was slightly increased, whereas the two functional properties related to site II were diminished and that to a pronounced degree.

3.3. In vivo studies

The time courses of radioactivity in rat plasma after intravenous administration of ^{125}I-labeled preparations of rHSA, the triple-residue mutant or glycated rHSA are shown in Fig. 5. It can be seen that glycated rHSA is eliminated more rapidly than the mutated rHSA which, in turn, is eliminated faster than rHSA. The eliminations of the proteins were characterized by examining merged α- and β-phases [34]. The lines for the three albumin forms in β-phases are essentially parallel, indicating similar metabolic half-lives, not differences in rate of elimination. The main difference among the three is the early fall, corresponding to the loss of albumin to extravascular spaces. Therefore, the mutated rHSA and the glycated rHSA might leave the circulation more rapidly and into larger spaces than the rHSA.

In order to examine the biological fate of the three albumin forms in more detail, we determined their liver and kidney uptake in mice. For these experiments, ^{111}In-labeling was preferred over ^{125}I-labeling. The advantage of the former method is that exchanges of ^{111}In chelating from labeled protein to other proteins in degradation space

Table 2
Hydrolysis rate constants (k_{obs}) for *p*-nitrophenyl acetate

rHSA	$10^3 \times k_{obs}$ (s^{-1})
Wild-type	9.05 ± 0.26
Triple-residue mutant	3.61 ± 0.18
Glycated wild-type (2.5 mM)	6.80 ± 0.13
(12.5 mM)	5.80 ± 0.09
(50 mM)	3.70 ± 0.14

The reaction mixtures contained 5 μM *p*-nitrophenyl acetate and 20 μM rHSA, triple-residue mutant or glycated rHSA in 67 mM sodium phosphate buffer (pH 7.4), and the reactions were followed at 25 °C. The values given are the means ± S.D. of three experiments. No activity of the medium by itself was observed.

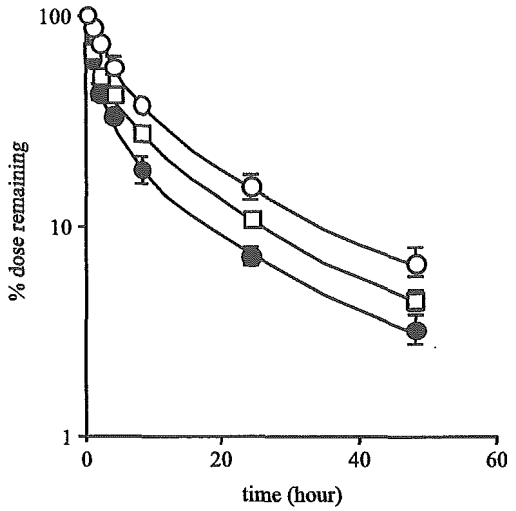

Fig. 5. Relative plasma levels of ^{125}I-labeled rHSA forms in rats after intravenous administration. ^{125}I-albumin was injected as a bolus through the vena cava superior of rats, and relative radioactivities are plotted against time after injection. rHSA (-○-), triple-residue mutant (-□-), and rHSA glycated with 50 mM glucose (-●-). Each data point represents the means ± S.D. for three rats.

results in a better target retention of radioactivity [23]. Thus, e.g. kidney uptake means association in kidney cells with or without degradation and not urine clearance. Table 3 shows that rHSA is little eliminated by liver and kidney and that both the mutation and glycation of rHSA result in very pronounced increments in liver and kidney uptake. Liver uptake increases by about 6-fold and 13-fold in both cases. Kidney uptake are also increased by the albumin modifications, but to a lesser degree than the liver uptake. Thus, the values for the mutated and the glycated proteins are increased about 1.6-fold and 2.4-fold, respectively. These findings suggest that most of the increased kidney uptake of the glycated protein could be caused by blockage of the three lysine residues. The finding that both the liver and the kidney uptake for glycated rHSA are higher than those for the mutated rHSA is in agreement with the findings of the rat experiments, i.e. the plasma half-life for glycated rHSA is lower than that for mutated rHSA.

The increased uptake of glycated rHSA in liver and kidneys is most probably due to the presence of cell membrane receptors which recognize the modified protein and internalize it by endocytosis. Hepatocytes and the nonparenchymal cells of the liver are involved in galactosyl receptor-mediated and mannose receptor-mediated endocytosis, respectively. Due to the specificities of these receptors, it is not likely that the increased liver clearance of glycated rHSA is caused by one of these mechanisms. It is more likely that the increased uptake is due to the presence of scavenger receptors in endothelial, Kupffer and parenchymal cells which are able to endocytose proteins with advanced glycation end products [35]. The results of the present study show that this type of liver uptake of albumin is partly due to the removal of positive charges on the surface of the protein. The uptake of the modified albumins by adsorptive endocytosis is assumed to be very low, because this type of uptake is dependent on the net positive charge of the protein [23].

Normally, glomerular filtration of albumin in the kidneys is followed by its return into the venous circulation without degradation (the albumin retrieval pathway). However, a small fraction is degraded in proximal tubular cells most probably after uptake by the endocytic receptor proteins megalin and cubilin [36]. Whether glycation results in an increased glomerular filtration and/or an increased uptake by this receptor-complex is not known. Glycated albumin could also simply be bound to the proximal tubular epithelial cells. An alternative explanation for the increased uptake of glycated rHSA could be the presence of tubular RAGE-receptors, which has been shown to cause the internalization of proteins with advanced glycation end products [37]. However, it has also been reported that albumin modified with Amadori-bound glucose, but not carbohydrate-free HSA, binds to calnexin, which is a mesangial cell receptor [38]. In any case, the kidney uptake clearance of glycated albumin was lower than that of liver (Table 3). In the kidneys, glycated proteins become degraded, and after degradation small soluble advanced glycation end product peptides are preferentially secreted into the glomerular filtrate and subsequently cleared by the kidneys [39].

Several reports have dealt with the effect of glycation on different aspects of albumin and other proteins. However, apparently nobody has examined whether possible effects are caused by protein binding of glucose or glucose-derived component(s) or by modification of amino acid residues per se. In this study, we have tried to shed some light on this question by using recombinant mutants of HSA. The results show that substituting three important lysines for alanines affects albumin in principally the same way as glycation. This finding proposes that the effect of glycation on the conformation, function and biological fate of HSA can, to a great extent, be explained by modification of, e.g. removal of the positive charges of lysine in positions 199, 439 and 525. However, the triple-residue mutant is not a perfect mimic for glycated HSA. The quantitative differences in the effects are likely to be due to the fact that glycation also affects arginine residues and additional lysine residues. Perhaps a perfect mimic for glycation can be made by mutating a proper combination of lysine and arginine residues. On the other hand, if that should indeed be

Table 3
Uptakes of rHSA forms by mice liver and kidneys

rHSA	Uptakes (μl/h)	
	Liver	Kidneys
Wild-type	6.90 ± 0.21	6.42 ± 0.41
Triple-residue mutant	41.64 ± 4.40	10.64 ± 1.47
Glycated wild-type (50 mM)	87.12 ± 7.20	15.44 ± 2.54

The values given are the means ± S.D. for three sets of experiments.

possible, it will support the conclusion of this study saying that the effect of glycation on structure, function and metabolism of HSA is primarily caused by blockage of positively charged amino acid residues.

Acknowledgements

This work was supported in part by Grants-in-Aid for Scientific Research from the Ministry of Education, Science, Sports and Culture of Japan (11694298; 11794016) and by Aarhus University Research Foundation.

References

[1] T. Peters Jr., All About Albumin: Biochemistry, Genetics, and Medical Applications, Academic Press, San Diego, 1996.
[2] X.M. He, D.C. Carter, Atomic structure and chemistry of human serum albumin, Nature 358 (1992) 209–215.
[3] S. Sugio, A. Kashima, S. Mochizuki, M. Noda, K. Kobayashi, Crystal structure of human serum albumin at 2.5 Å resolution, Protein Eng. 12 (1999) 439–446.
[4] E. Bourdon, N. Loreau, D. Blache, Glucose and free radicals impair the antioxidant properties of serum albumin, FASEB J. 13 (1999) 233–244.
[5] H. Vorum, K. Fisker, M. Otagiri, A.O. Pedersen, U. Kragh-Hansen, Calcium ion binding to clinically relevant chemical modifications of human serum albumin, Clin. Chem. 41 (1995) 1654–1661.
[6] N. Shaklai, R.L. Garlick, H.F. Bunn, Nonenzymatic glycosylation of human serum albumin alters its conformation and function, J. Biol. Chem. 259 (1984) 3812–3817.
[7] N. Iberg, R. Fluckiger, Nonenzymatic glycosylation of albumin in vivo. Identification of multiple glycosylated sites, J. Biol. Chem. 261 (1986) 13542–13545.
[8] D.A. Robb, O.S. Olufemi, D.A. Williams, J.M. Midgley, Identification of glycation at the *N*-terminus of albumin by gas chromatography-mass spectrometry, Biochem. J. 261 (1989) 871–878.
[9] R.F. Chen, Removal of fatty acids from serum albumin by charcoal treatment, J. Biol. Chem. 242 (1967) 173–181.
[10] H. Watanabe, K. Yamasaki, U. Kragh-Hansen, S. Tanase, K. Harada, A. Suenaga, M. Otagiri, In vitro and in vivo properties of recombinant human serum albumin from *Pichia pastoris* purified by a method of short processing time, Pharm. Res. 18 (2001) 1775–1781.
[11] P.J. Coussons, J. Jacoby, A. McKay, S.M. Kelly, N.C. Price, J.V. Hunt, Glucose modification of human serum albumin: a structural study, Free Radic. Biol. Med. 22 (1997) 1217–1227.
[12] M. Rendell, P.M. Stephen, R. Paulsen, J.L. Valentine, K. Rasbold, T. Hestorff, S. Eastberg, D.C. Shint, An interspecies comparison of normal levels of glycosylated hemoglobin and glycosylated albumin, Comp. Biochem. Physiol. 81B (1985) 819–822.
[13] R. Nagai, K. Matsumoto, X. Ling, H. Suzuki, T. Araki, S. Horiuchi, Glycolaldehyde, a reactive intermediate for advanced glycation end products, plays an important role in the generation of an active ligand for the macrophage scavenger receptor, Diabetes 49 (2000) 1714–1723.
[14] H. Watanabe, U. Kragh-Hansen, S. Tanase, K. Nakajou, M. Mitarai, Y. Iwao, T. Maruyama, M. Otagiri, Conformational stability and warfarin-binding properties of human serum albumin studied by recombinant mutants, Biochem. J. 357 (2001) 269–274.
[15] N. Muller, F. Lapicque, E. Drelon, P. Netter, Binding sites of fluorescent probes on human serum albumin, J. Pharm. Pharmacol. 46 (1994) 300–304.
[16] V. Maes, Y. Engelborghs, J. Hoebeke, Y. Maras, A. Vercruysse, Fluorimetric analysis of the binding of warfarin to human serum albumin. Equilibrium and kinetic study, Mol. Pharmacol. 21 (1982) 100–107.
[17] K.M. Rajkowski, Comparison of graphical procedures for estimating the intrinsic molar fluorescence of protein-bound drugs for drug-binding studies. A reevaluation of existing plots and introduction of two inverse hyperbolic plots, Biochem. Pharmacol. 39 (1990) 895–900.
[18] Y. Ozeki, Y. Kurono, T. Yotsuyanagi, K. Ikeda, Effects of drug binding on the esterase activity of human serum albumin: inhibition modes and binding sites of anionic drugs, Chem. Pharm. Bull. 28 (1980) 535–540.
[19] Y. Kurono, I. Kushida, H. Tanaka, K. Ikeda, Esterase-like activity of human serum albumin: VIII. Reaction with amino acid *p*-nitrophenyl esters, Chem. Pharm. Bull. 40 (1992) 2169–2172.
[20] W.M. Hunter, F.C. Greenwood, Preparation of iodine-131 labeled human growth hormone of high specific activity, Nature 194 (1962) 495–496.
[21] D.J. Hnatowich, W.W. Layne, R.L. Childs, The preparation and labeling of DTPA-coupled albumin, Int. J. Appl. Radiat. Isot. 33 (1982) 327–332.
[22] T. Mukai, Y. Arano, K. Nishida, H. Sasaki, H. Saji, J. Nakamura, In vivo evaluation of Indium-111-diethylenetriaminepentaacetic acid-labelling for determining the sites and rates of protein catabolism in mice, J. Pharm. Pharmacol. 51 (1999) 15–20.
[23] F. Staud, M. Nishikawa, K. Morimoto, Y. Takakura, M. Hashida, Disposition of radioactivity after injection of liver-targeted proteins labeled with ^{111}In or ^{125}I. Effect of labelling on distribution and excretion of radioactivity in rats, J. Pharm. Sci. 88 (1999) 577–585.
[24] P.R. Smith, P.J. Thornalley, Mechanism of the degradation of non-enzymatically glycated proteins under physiological conditions. Studies with the model fructosamine, *N*-epsilon-(1-deoxy-D-fructos-1-yl)hippuryl-lysine, Eur. J. Biochem. 210 (1992) 729–739.
[25] M.P. Heyes, C.Y. Chen, E.O. Major, K. Saito, Different kynurenine pathway enzymes limit quinolinic acid formation by various human cell types, Biochem. J. 326 (1997) 351–356.
[26] Y. Sreelakshmi, K.K. Sharma, Interaction of alpha-lactalbumin with mini alphaA-crystallin, J. Protein Chem. 20 (2001) 123–130.
[27] M. Anraku, K. Yamasaki, T. Maruyama, U. Kragh-Hansen, M. Otagiri, Effect of oxidative stress on the structure and function of human serum albumin, Pharm. Res. 18 (2001) 632–639.
[28] C.E. Petersen, C.E. Ha, S. Curry, N.V. Bhagavan, Probing the structure of the warfarin-binding site on human serum albumin using site-directed mutagenesis, Proteins 47 (2002) 116–125.
[29] N. Ahmed, P.J. Thornalley, Chromatographic assay of glycation adducts in human serum albumin glycated in vitro by derivatization with 6-aminoquinolyl-*N*-hydroxysuccinimidyl-carbamate and intrinsic fluorescence, Biochem. J. 364 (2002) 15–24.
[30] P.J. Thornalley, A. Langborg, H.S. Minhas, Formation of glyoxal, methylglyoxal and 3-deoxyglucosone in the glycation of proteins by glucose, Biochem. J. 344 (1999) 109–116.
[31] H. Watanabe, S. Tanase, K. Nakajou, T. Maruyama, U. Kragh-Hansen, M. Otagiri, Role of Arg-410 and Tyr-411 in human serum albumin for ligand binding and esterase-like activity, Biochem. J. 349 (2000) 813–819.
[32] N. Okabe, N. Hashizume, Drug binding properties of glycosylated human serum albumin as measured by fluorescence and circular dichroism, Biol. Pharm. Bull. 17 (1994) 16–21.
[33] J.P. Bohney, R.C. Feldhoff, Effects of nonenzymatic glycosylation and fatty acids on tryptophan binding to human serum albumin, Biochem. Pharmacol. 43 (1992) 1829–1834.
[34] J.W. Baynes, S.R. Thorpe, Identification of the sites of albumin catabolism in the rat, Arch. Biochem. Biophys. 206 (1981) 372–379.
[35] B. Smedsrod, J. Melkko, N. Araki, H. Sano, S. Horiuchi, Advanced

glycation end products are eliminated by scavenger-receptor-mediated endocytosis in hepatic sinusoidal, Kupffer and endothelial cells, Biochem. J. 322 (1997) 567–573.
[36] E.I. Christensen, H. Birn, Megalin and cubilin: synergistic endocytic receptors in renal proximal tubule, Am. J. Physiol., Renal Physiol. 280 (2001) F562–F573.
[37] A. Abiko, M. Eto, I. Makino, N. Araki, S. Horiuchi, Increased levels of advanced glycosylation end products in the kidney and liver from spontaneously diabetic Chinese hamsters determined by immunochemical assay, Metabolism 49 (2000) 567–573.
[38] V.Y. Wu, C.W. Shearman, M.P. Cohen, Identification of calnexin as a binding protein for Amadori-modified glycated albumin, Biochem. Biophys. Res. Commun. 284 (2001) 602–606.
[39] R. Singh, A. Barden, T. Mori, L. Beilin, Advanced glycation end-products: a review, Diabetologia 44 (2001) 129–146.

0022-3565/03/3073-1234–1242$7.00
THE JOURNAL OF PHARMACOLOGY AND EXPERIMENTAL THERAPEUTICS
Copyright © 2003 by The American Society for Pharmacology and Experimental Therapeutics
JPET 307:1234–1242, 2003

Vol. 307, No. 3
56499/1108104
Printed in U.S.A.

Evidence for the Involvement of a Pulmonary First-Pass Effect via Carboxylesterase in the Disposition of a Propranolol Ester Derivative after Intravenous Administration

TERUKO IMAI, YASUSHI YOSHIGAE, MASAKIYO HOSOKAWA, KAN CHIBA, and MASAKI OTAGIRI

Faculty of Pharmaceutical Sciences, Kumamoto University, Kumamoto, Japan (T.I., Y.Y., M.O.); and Faculty of Pharmaceutical Sciences, Chiba University, Chiba, Japan (M.H., K.C.)

Received July 3, 2003; accepted August 21, 2003

ABSTRACT

The disposition kinetics of *O*-butyryl propranolol (butyryl-PL), a model compound containing an ester moiety, after intravenous administration was compared with that of PL in rats and beagle dogs. Rats showed only 30% conversion of butyryl-PL to PL up to 2 h after dosing, whereas dogs showed nearly complete conversion within 10 min after administration. The CL_{total} of butyryl-PL in rats was 5.8 l/h/kg and that in dogs was 65.6 ± 18.6 l/h/kg, both of which were greater than hepatic blood flow. The in vivo conversion from butyryl-PL to PL in the rat could be explained on the basis of the hydrolysis characteristics in the liver and blood. The in vitro hydrolysis data and the in vivo data after intra-arterial administration clearly demonstrated that the extremely high CL_{total} of butyryl-PL in dogs was dependent on first-pass hydrolysis in the lung in addition to hydrolysis at a blood flow-limited rate in the liver and kidney. The availability of butyryl-PL after passage through the lung was 50%. Furthermore, the isoform of carboxylesterase involved in the pulmonary hydrolysis of butyryl-PL in the dog was identified as D1, a CES-1 group enzyme. However, butyryl-PL was not recognized as a substrate by CES-1 family carboxylesterases, which are present at high levels in the rat lung (RH-1) and kidney (RL-1). These findings indicate that extrahepatic metabolism, especially in the lung, is important in the disposition of drugs containing an ester moiety after intravenous administration and that the substrate specificity of carboxylesterase isozyme distinguishes from others.

A number of ester- and amide-containing drugs have been clinically used in oral, cutaneous, and injectable formulations. The main route of detoxification or metabolic activation of these compounds is through enzymatic hydrolysis. Multiple carboxylesterases (E.C. 3.1.1.1) efficiently catalyze the hydrolysis of ester- and amide-containing drugs to their respective free acids, and these carboxylesterases are localized in the endoplasmic reticulum (ER) of a variety of organs and tissues in many mammalian species (Heymann, 1982; Satoh, 1987; Satoh and Hosokawa, 1998). In general, marked species differences are seen in esterase activity. For example, the level of esterase activity in mammalian liver microsomes is in the order dog > human > rat when *p*-nitrophenylacetate is used as the substrate, but is in the order dog > rat > human for isocarboxazid (Hosokawa et al., 1990). The different spectra of esterase activity for different substrates in various tissues lead to markedly divergent patterns of disposition after the administration of ester- and amide-containing drugs via various routes in mammalian species. Of all the animal tissues studied to date, the highest level of hydrolase activity is seen in the liver and a moderate level of hydrolase activity is seen in the proximal tubule of the kidney (Tsujita et al., 1988; Tsujita and Okuda, 1993). Interestingly, significant esterase activity has recently been found in the small intestine (Prueksaritanont et al., 1996; Yoshigae et al., 1998b), the skin (McCracken et al., 1993; Ahmed et al., 1997), the heart (Dean et al., 1995), muscle (Nambu et al., 1987), the blood (Van Lith et al., 1992; McCracken et al., 1993; Ahmed et al., 1997), and the lung (McCracken et al., 1993; Dean et al., 1995; Forkert et al., 2001). Although hydrolase activity is observed in most tissues, ester- and amide-containing drugs are converted to free acid mainly by the hydrolase activity in the liver. Moreover, further metabolism in various organs complicates the disposition of drugs after administration to animals.

The present study focused on the extrahepatic metabolism by esterase, particularly pulmonary metabolism, as well as species differences in metabolism, using *O*-butyryl-propranolol (butyryl-PL; Fig. 1), a PL ester derivative, as a model

Article, publication date, and citation information can be found at http://jpet.aspetjournals.org.
DOI: 10.1124/jpet.103.056499.

ABBREVIATIONS: ER, endoplasmic reticulum; PL, propranolol; HPLC, high-performance liquid chromatography; Rb, blood/plasma ratio; AUC, area under the curve; CL, clearance; BNPP, bis-nitrophenyl phosphate; DMSO, dimethyl sulfoxide; PAGE, polyacrylamide gel electrophoresis; P450, cytochrome P450; PNPA, *p*-nitrophenylacetate.

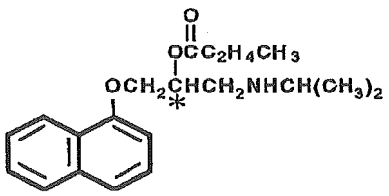

O-Butyryl Propranolol
(Butyryl-PL)

Fig. 1. Structure of butyryl-PL.

ester-containing compound. PL is distributed not only to the liver but also to several other tissues, including the lung, due to its hydrophobicity and basicity. Pang et al. (1982) has reported 50 to 60% first-pass uptake of PL by the lung through a simple diffusion mechanism in dogs with cardiac catheterization. Dollery and Junod (1976) have reported the accumulation of PL in the rat lung. Butyryl-PL is more hydrophobic than PL and its basicity is comparable with that of PL [$\log P_{(n\text{-octanol/pH 4.0 buffer})}$: PL, 0.38; butyryl-PL, 1.54; and pK_a: PL, 9.44; butyryl-PL, 9.02]. Therefore, it is possible that butyryl-PL may be easily taken up and hydrolyzed to PL in the lung after intravenous administration.

In the present study, the disposition kinetics of butyryl-PL after intravenous administration was investigated in rats and beagle dogs. The tissues contributory to the hydrolysis of butyryl-PL were also identified in these two species. In addition, the extent of in vivo hydrolase activity in the lung was determined by comparison of intravenous and intra-arterial administration of butyryl-PL in beagle dogs. Furthermore, the isoform of carboxylesterase involved in pulmonary hydrolysis of butyryl-PL in the dog was identified.

Materials and Methods

Materials. *O*-butyryl-PL hydrochloride was synthesized from PL hydrochloride (Wako Pure Chemicals, Osaka, Japan) and butyryl chloride (Tokyo Kasei, Tokyo, Japan) according to the methods described previously (Shameem et al., 1993). The identity and purity of the synthesized butyryl-PL were confirmed by infrared, NMR, atomic analysis, and HPLC. All other reagents used were of analytical grade.

Intravenous Administration to Rats and Beagle Dogs. Male Wistar rats (230–270 g, 8 weeks of age) and beagle dogs (9–11 kg, 1–3 years of age) were housed in an air-conditioned room with free access to commercial chow and tap water, and fasted for 15 h before the intravenous administration of PL or butyryl-PL. PL (2.5 mg/400 μl/kg for rats, 2.0 mg/400 μl/kg for dogs), and equivalent doses of butyryl PL were dissolved in sterilized phosphate buffer (0.05 M, pH 6.0). In rats, the solutions were injected via the femoral vein and blood samples were drawn from the jugular vein under ether anesthesia. In dogs, the solutions were injected via the right cephalic vein and blood samples were drawn from the left cephalic vein without anesthesia.

Intra-Arterial Administration of Butyryl-PL to Beagle Dogs. Before intra-arterial administration to beagle dogs, a catheter (pig-tail angiocatheter; Goodman Co., Ltd. Nagoya, Japan) was advanced via the femoral artery until the tip was placed in the left ventricle. The dogs were anesthetized by the intramuscular injection of atropine (0.005 mg/kg; Fuso Pharmaceutical Industry Ltd., Osaka, Japan), and further intramuscular injection of mixture of ketamine hydrochloride (0.66 mg/kg; Sankyo Co., Ltd., Tokyo, Japan) and Xylazin hydrochloride (0.13 mg/kg; Bayer AG, Leverkusen, Germany). Proper placement of the catheter in the left ventricle was confirmed by monitoring the blood pressure. Four hours after arousal, butyryl-PL was injected into the left ventricle via the intra-arterial catheter. The butyryl-PL solution was the same as that used for i.v. injection (2 mg/400 μl/kg equivalent to PL). The catheter was flushed with phosphate-buffered saline solution (pH 6.0) to ensure that no butyryl-PL remained in the catheter before it was removed from the femoral artery.

Determination of Plasma Concentrations of PL and Butyryl-PL. Blood samples (0.45 ml for rats, 1.0 ml for dogs) were drawn using heparinized syringes rinsed with a trace amount of paraoxon, an inhibitor of the hydrolysis of butyryl-PL. The plasma sample (200 μl) obtained from each blood sample after centrifugation (12,000*g* for 30 s) was added to 0.3 ml of 0.1 M phosphate buffer (pH 4.0) saturated with NaCl. PL and butyryl-PL were then simultaneously extracted twice with 6 ml of ethyl acetate. Less than 1% of the butyryl-PL in the plasma degraded by after this procedure. The organic phase was evaporated to dryness and the residual material was redissolved in 50 μl of the mobile phase before the injection of a 20-μl aliquot into the HPLC system.

Data Analysis for Blood Concentrations of PL and Butyryl-PL. The blood level of each compound was calculated from the plasma concentration based on the blood/plasma ratio (Rb). The Rb was estimated from the drug concentrations in the plasma and blood after incubation of each compound in the blood, which was treated with 1 μM paraoxon, for 10 min at 37°C. The mean Rb values of PL and butyryl-PL were constant over the concentration range from 10 to 1000 ng/ml. In addition, the Rb values of PL and butyryl-PL immediately after adding them in the blood were nearly same as those after 10-min incubation. In rats, the Rb of (*R*)-PL and (*S*)-PL was 0.55 and 1.2, respectively, and that of butyryl-PL was 0.88 for (*R*)-isomer and 0.91 for (*S*)-isomer. In dogs, the Rb of both (*R*)- and (*S*)-PL was 0.80, and that of butyryl-PL for both enantiomers was also 0.80. The racemic blood levels of PL and butyryl-PL were calculated as the sum of the blood concentrations of each enantiomer. The AUC from time 0 to infinity ($AUC_{0-\infty}$) was calculated as the sum of the AUC of the mean blood concentration-time curve up to final sampling point by the trapezoidal rule and the AUC from the terminal exponential slope obtained by linear regression of the log-linear portion of the blood concentration profile. The apparent total body clearance was calculated as dose/$AUC_{0-\infty}$.

Organ clearance (CL_{org}) for liver and kidney was calculated by following equation: $CL_{org} = Q \cdot f_b \cdot CL_{int}/(Q + f_b \cdot CL_{int})$. Pulmonary clearance was calculated from $CL_{org} = f_b \cdot CL_{int}$. Intrinsic clearance ($CL_{int}$, liters per hour per kilogram) was estimated from the Michaelis-Menten kinetic parameters and protein content (milligrams per kilogram body) in respective organ according to the following equation: $CL_{int} = (V_{max}/K_m) \times$ (protein content), where protein content was 1,280 mg/kg for rat liver microsomes, 3,218 mg/kg for dog liver S9, 425 mg/kg for dog lung S9, and 423 mg/kg for dog kidney S9. The free fraction in blood (f_b) for butyryl-PL was calculated by f_p/Rb. The free fraction of butyryl–PL in plasma (f_p) treated with 1 μM paraoxon was determined by ultrafiltration method using a micropartition system MPS-1 (Amicon, Danvers, MA; a molecular weight cut-off value of 30,000). The f_p value of racemic butyryl-PL was 0.08 for rats and 0.07 for dogs. Then, f_b of butyryl-PL was calculated 0.09 for both dogs and rats. Tissue blood flow rate (Q) listed in Table 3 was used for calculation.

A deconvolution method (Prueksaritanont et al., 1997) was used to calculate the systemic formation rate of PL after intravenous administration of butyryl-PL. Assuming that the disposition kinetics of PL and butyryl-PL was independent of each other and that their disposition kinetics were linear, the systemic formation rate (Rm) was calculated by following equation:

$$C_{Bu\rightarrow PL}(t) = \int_0^t Rm(\tau) \cdot C_{PL}(t-\tau) d\tau$$

where Rm is the systemic formation rate of PL from butyryl-PL, $C_{Bu\rightarrow PL}$ and C_{PL} are plasma PL concentration after intravenous administration of butyryl-PL and PL.

Preparation of Microsomes and Cytosol from Various Organs. Male beagle dogs (9–10 kg, 4–5 years of age) and male Wistar rats (230–270 g, 8 weeks of age) were used after overnight fasting with free access to water. The dogs and rats were sacrificed by exsanguination under ether anesthesia. A cannula was place in the inferior vena cava, and the liver, kidneys, and lungs were perfused with ice-cold 0.15 M KCl to remove the blood. These organs were then resected, washed with ice-cold 0.15 M KCl, and homogenized with 3 volumes of 10 mM phosphate buffer (pH 7.4) containing 0.15 M KCl in a Potter-Elvehjem glass homogenizer equipped with a Teflon pestle under ice-cold conditions. The microsomes and cytosol fractions were prepared as described previously (Yoshigae et al., 1997). Briefly, the homogenate obtained (25% wet w/v) was centrifuged at 9000*g* for 20 min at 4°C to obtain the supernatant (S9) fraction. The S9 fraction was further centrifuged at 105,000*g* for 1 h at 4°C, and the resulting supernatant was used as the cytosolic fraction. The pellets were washed and resuspended by homogenization in phosphate buffer to obtain the microsomes solution. Protein content was determined by the method of Lowry et al. (1951) using bovine serum albumin as the standard protein, and the enzyme solutions were stored at −80°C until use.

Hydrolysis Experiments. Hydrolysis experiments were performed using subcellular fractions diluted with Tris-HCl buffer (50 mM, pH 7.4) according to the method described previously (Yoshigae et al., 1997). The hydrolysis reaction was initiated by the addition of butyryl-PL after preincubation of each subcellular fraction for 5 min. The reaction was terminated by the addition of acetonitrile. In experiments involving inhibition by bis-*p*-nitrophenyl phosphate (BNPP), the enzyme solution was preincubated for 5 min with various concentrations of BNPP (final concentrations, 10^{-8}–10^{-3} M) dissolved in dimethyl sulfoxide (DMSO; 5 μl) or without esterase inhibitor (5 μl of DMSO alone) in controls. DMSO, a solvent for butyryl-PL and BNPP, was added to a final concentration of 1% (v/v) in the enzyme solution. The PL formed was determined by HPLC.

HPLC Assay for Enantiomers of PL and Butyryl-PL. The HPLC assay was performed according to method described previously (Yoshigae et al., 1998a). The HPLC system comprised a Hitachi L-6000 pump with a loop-fitted Rheodine injector (volume 20 μl), a Hitachi L-7480 fluorescence detector, and a Hitachi D-2500 chromato-integrator (Hitachi Co., Ltd., Tokyo, Japan). In the case of butyryl-PL, an ES-PhCD column (150 × 6.0-mm i.d.; Shinwa Chemical Industries, Ltd., Kyoto, Japan) was used with a mobile phase of acetonitrile/20 mM KH_2PO_4 [45:55 (v/v)] at a flow rate of 0.8 ml/min. A Chiralcel OD column (25 × 0.46-cm i.d.; Daisel Chemical Industries, Ltd., Tokyo, Japan) was used for PL with a mobile phase of *n*-hexane/ethanol/diethylamine [85:15:0.6 (v/v/v)] at a flow rate of 0.6 ml/min. Both PL and butyryl-PL were detected with excitation and emission wavelengths of 285 and 340 nm, respectively.

Inhibition Experiments for Hydrolysis Using anti-D1 Polyclonal Antibody. Anti-D1 polyclonal IgG was purified from anti-D1 rabbit serum using a Protein D column (Funakoshi, Tokyo, Japan) eluted with phosphate buffer (pH 3.0) containing 100 mM glycine. Microsomes from rat and dog tissues were incubated with anti-D1 IgG for 30 min at 37°C in Tris-HCl buffer (pH 7.4). The mixtures were allowed to stand overnight at 4°C and then centrifuged at 10,000*g* for 5 min. The resulting supernatant was used to assay hydrolase activity for butyryl-PL. The inhibition of activity by the antibody was calculated as the percentage of control activity using control rabbit IgG (Bayer AG).

Polyacrylamide Gel Electrophoresis. Polyacrylamide gel electrophoresis (PAGE) was performed as described by Mentlein et al. (1980). Polyacrylamide gels [7.5% (w/w)] containing 1% (w/v) Nonidet P-40 for solubilization of proteins were used for the separation of native enzymes. After electrophoresis of the microsomal and cytosol samples (35–130 μg of protein), the gels were stained for esterase activity with 1-naphthylbutyrate through coupling to liberated 1-naphthol with Fast Red TR-salt.

Immunochemical staining was carried out according to the method described previously (Hosokawa et al., 1987). Briefly, after SDS-PAGE was performed, the denaturing proteins were transferred from the acrylamide gels to a nitrocellulose membrane for 1 h using an Atto semidry transfer unit (Atto Co., Tokyo, Japan). The membrane was blocked for 1 h with 1.5% (w/v) bovine serum albumin solution in blocking buffer [0.1% (w/v) Tween 20, 25 mM Tris pH 7.4, and 150 mM NaCl]. After the membrane was incubated with rabbit anti-D1 IgG for 1 h, the membrane was rinsed three times with blocking buffer and was then incubated with goat antibody to rabbit IgG for 1 h. After washing with blocking buffer, the membrane was processed using a Konica immuno-detection system for determining peroxidase activity (Konica Co., Ltd., Tokyo, Japan).

Results

Blood Concentrations of PL and Butyryl-PL after Intravenous Administration. The plasma levels of PL and butyryl-PL after intravenous administration of PL and butyryl-PL to rats (2.5 mg/kg, equivalent to PL) and dogs (2.0 mg/kg, equivalent to PL) are shown in Fig. 2. After the intravenous administration of butyryl-PL to rats, the plasma concentrations of both intact butyryl-PL and converted PL were significantly lower than the plasma PL concentration from intravenously administered PL. In contrast, the temporal profile of PL converted from butyryl-PL after the intravenous administration of butyryl-PL in dogs was nearly the same as that of the intravenously administered PL, although the plasma concentration of intact butyryl-PL was markedly lower.

The apparent hydrolysis ratio from butyryl-PL to PL after intravenous administration was analyzed using the deconvolution method. The plasma levels of PL after the administration of butyryl-PL and after the administration of PL were used as the output and weight functions, respectively. The results of the analysis showed that only 30% of the butyryl-PL was converted to PL up to 2 h after administration in rats, whereas nearly complete conversion was observed within 10 min in beagle dogs (Fig. 3).

The AUC_{blood} and CL_{total} of PL and butyryl-PL after intravenous administration in rats and dogs are listed in Table 1. In both species, the CL_{total} for PL was nearly the same as the hepatic blood flow due to high clearance via hepatic P450 metabolism, which in agreement with the findings of previous reports (George et al., 1976; Iwamoto and Watanabe, 1985). However, the CL_{total} of butyryl-PL in rats was about 1.5-fold greater than hepatic blood flow, and dogs showed a significantly increased CL_{total}, that was about 35-fold greater than hepatic blood flow and about 9-fold greater than cardiac output. In both species, particularly in the dog, the CL_{total} exceeded hepatic blood flow, indicating that extrahepatic metabolism contributed to the elimination of butyryl-PL.

In Vitro Hydrolysis in Rat and Dog Tissues. In general, the liver is the most efficient organ for drug metabolism, but other organs such as the lung and kidney also often exhibit considerable drug metabolism activity. Moreover, high esterase activity is also present in the plasma. Therefore, the hydrolase activity for butyryl PL in these tissues was assayed to clarify the extrahepatic metabolism of butyryl-PL. As shown in Table 2, the highest esterase activity for butyryl-PL in rats was observed in the liver microsomes, in contrast to significantly lower activities in the liver cytosol and in the lung and kidney preparations. The hydrolase activity of lung and kidney microsomes was more than 60

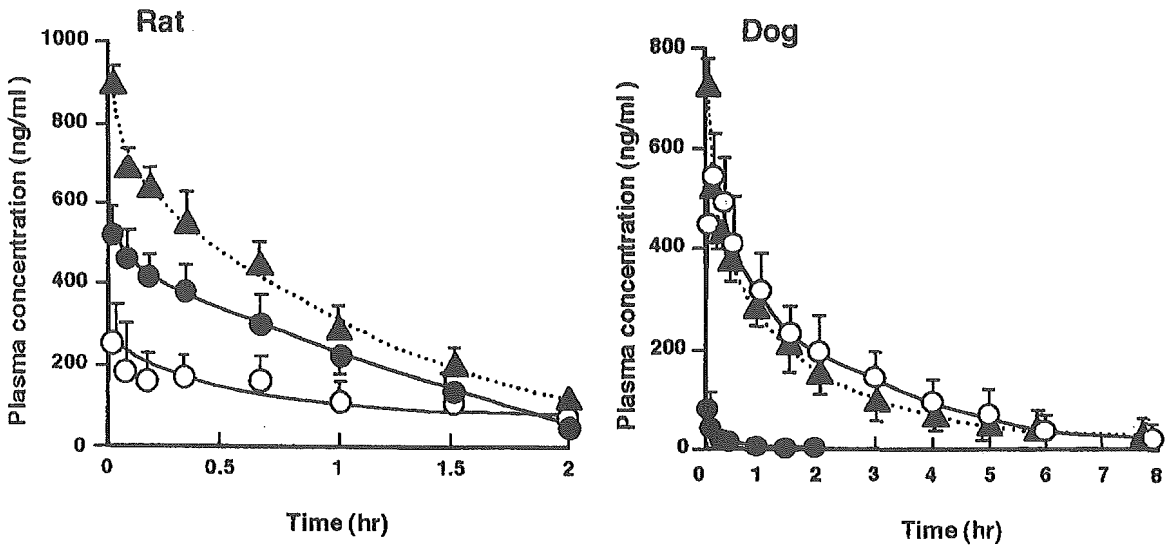

Fig. 2. Plasma concentrations of PL and butyryl-PL after intravenous administration of PL and butyryl-PL in rats and dogs (2.5 mg/kg for rats and 2.0 mg/kg for dogs, equivalent to PL). Symbols indicate PL administration (▲), butyryl-PL (●), and PL (○) after butyryl-PL administration. Values are mean ± S.D. (n = 4).

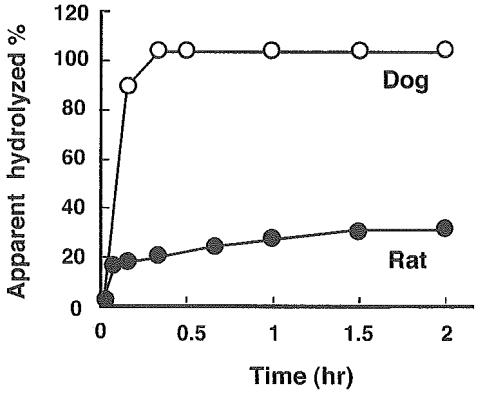

Fig. 3. Apparent hydrolysis ratio of butyryl-PL after intravenous administration to rats (●) and dogs (○). The hydrolysis ratio was calculated by the deconvolution method. The plasma PL concentration profiles after intravenous administration of butyryl-PL and PL were used as the output function and weight function, respectively.

TABLE 1

AUC_{blood} and CL_{total} of PL and butyryl-PL after intravenous administration in rats and dogs

Dosing Compound	Rat[a]	Dog
PL		
$AUC_{blood,PL}$ (ng · h/ml)	649	1052 ± 219
$CL_{total,PL}$ (l/h/kg)	3.85	1.90 ± 0.61
Butyryl-PL		
$AUC_{blood,Bu}$ (ng · h/ml)	433	30.5 ± 8.60
$AUC_{blood,Bu\rightarrow PL}$ (ng · h/ml)	289	1103 ± 310
$CL_{total,Bu}$ (l/h/kg)	5.77	65.6 ± 18.6
Blood flow (l/h/kg)		
Liver	3.6	1.9
Cardiac output	17.8	7.2

[a] Parameters were calculated from mean blood concentration after intravenous administration of PL and butyryl-PL in rats (2.5 mg/kg for rats, equivalent to PL). AUC of drugs after administration in rats was calculated from mean plasma concentrations from time zero to infinity. AUC_{blood} = AUC_{plasma} × Rb. $AUC_{blood,PL}$ means the AUC_{blood} of PL after administration of PL. $AUC_{blood,Bu}$ and $AUC_{blood,Bu\rightarrow PL}$ mean the AUC_{blood} of butyryl-PL and PL after administration of butyryl-PL, respectively. $CL_{total,PL}$ and $CL_{total,Bu}$ mean the total clearance of PL and butyryl-PL after administration of PL and butyryl-PL, respectively.

times lower than that of liver microsomes. However, high levels of hydrolase activity for p-nitrophenylacetate (PNPA), a substrate for carboxylesterase, were observed in liver, kidney, and lung microsomes. These findings suggest that butyryl-PL is not easily recognized by the esterases in the rat lung and kidney.

On the other hand, dogs showed high hydrolase activity not only in the liver but also in the lung and the kidney, as shown in Table 2. The hydrolase activity in several organs (except for the plasma) was much higher in dogs than in rats. Although the order of hydrolase activity for butyryl-PL was liver > kidney ≥ lung, that for PNPA was liver ≥ lung > kidney. These findings suggest that substrate specificity varies in different tissues, possibly due to the expression of different esterases.

In addition, the hydrolase activity of rat plasma for butyryl-PL was 187 ± 11.4 pmol/min/mg protein, which seemed quite low compared with that of liver microsomes. This may have been due to a high protein content of plasma proteins such as albumin. In fact, the hydrolysis half-life of butyryl-PL (100 μM, 43.5 μg/ml) was about 4 min in rat plasma and 2.8 min in rat blood. In contrast, the hydrolase activity for butyryl-PL in dog plasma was 18.8 ± 2.71 pmol/min/mg protein and its half-life was about 70 min. In addition, the hydrolysis half-life of butyryl-PL in the blood was 31 min, which was much shorter than that in plasma due to contribution of red blood cells to hydrolysis. However, the hydrolysis half-life of butyryl-PL in dog blood is markedly longer than the in vivo elimination half-life of butyryl-PL.

Estimation of Organic Clearance from in Vitro Hydrolysis Parameters. The enzyme kinetic parameters, K_m and V_{max}, for hydrolase activity in tissue microsomes were estimated, and the organic clearance was then calculated from the K_m and V_{max} values based on a well stirred model (Table 3). The hepatic clearance of butyryl-PL in rat was nearly the same as the hepatic blood flow, indicating that butyryl-PL was hydrolyzed at a hepatic blood flow-limited rate in the rat liver. However, hepatic clearance accounted for only 60% of the CL_{total} after intravenous administration in the rat. The remaining 40% of the CL_{total} may have been due mainly to hydrolysis in the blood, showing a short half-life of 2.8 min, because hydrolase activity is quite low in the rat kidney and lung.

TABLE 2
Hydrolysis activity of plasma, liver, lung, and kidney

Tissue	Rat			Dog		
	Total Activity for *R*- and *S*- Butyryl-PL	*R/S* Ratio	Activity for PNPA	Total Activity for *R*- and *S*-Butyryl-PL	*R/S* Ratio	Activity for PNPA
Plasma (pmol/min/mg protein)	187 ± 11.4	1.13		18.8 ± 2.71	5.36	
Liver (nmol/min/mg protein)						
Microsomes	172 ± 25.4	0.39	3550 ± 733	363 ± 35.5	2.59	6750 ± 276
Cytosol	1.47 ± 0.26	0.49		109 ± 19.87	3.78	
Lung (nmol/min/mg protein)						
Microsomes	1.93 ± 0.08	2.39	350 ± 35.7	131 ± 7.37	3.08	6130 ± 357
Cytosol	1.64 ± 0.17	1.59		43.3 ± 5.30	3.04	
Kidney (nmol/min/mg protein)						
Microsomes	2.78 ± 0.19	0.40	928 ± 138	183 ± 10.8	2.80	1820 ± 48.9
Cytosol	1.36 ± 0.09	0.87		16.2 ± 0.59	1.94	

Organic clearance in dogs was estimated from the hydrolase activity in the S9 fraction due to the presence of hydrolase activity in both the micosome and cytosol fractions. The CL_{organ} of the liver was the same as the hepatic blood flow, indicating that butyryl-PL was hydrolyzed at hepatic blood flow-limited rate in the dog liver. The CL_{organ} values of the lung and kidney were also high at 60 and 70% of the blood flow rate, respectively. Interestingly, the lung showed the highest CL_{organ} among these three organs. However, the in vivo CL_{total} (65.6 l/h/kg) was much higher than the sum of the CL_{organ} values of these three organs (7.3 l/h/kg). In general, an intravenously administered drug first enters the lung and is then distributed to the other organs via arterial blood flow. The above-mentioned findings suggest that butyryl-PL is hydrolyzed by the first-pass effect through the lung before entering the systemic circulation in beagle dogs.

Intra-Arterial Administration of Butyryl-PL to Dogs. To demonstrate the extent of first-pass hydrolysis in the dog lung, butyryl-PL was administered intracardially as a route of administration that bypasses the lungs. Figure 4 shows that the plasma concentrations of PL converted from butyryl-PL after intra-arterial administration were significantly lower than those after intravenous administration. The AUCs of intact butyryl-PL after intra-arterial and intravenous administration of butyryl-PL were 67.1 ± 28.7 and 30.5 ± 8.6 ng · h/ml, respectively, and their ratio (indicating availability of butyryl-PL after passage through the lung) was about 50%. These findings indicate that butyryl-PL undergoes first-pass hydrolysis in the lung in beagle dogs.

TABLE 3
Enzyme kinetic parameters of rat liver microsomes and dog liver, lung, and kidney 9000g supernatants for butyryl-PL and its CL_{org} estimated from in vitro data

Tissue[a]	K_m	V_{max}	CL_{int}[b]	CL_{org}[c]	Q
	μM	*nmol/min/mg protein*		*l/h/kg*	
Rat					
Liver	180 ± 21.8	709 ± 19.3	304 ± 27.5	3.3	3.6
Dog					
Liver	62.5 ± 0.60	292 ± 10.0	901 ± 37.3	1.9	1.9
Lung	65.3 ± 10.4	120 ± 14.4	50.1 ± 7.01	4.5	7.2
Kidney	132 ± 22.6	180 ± 30.7	34.7 ± 4.10	0.9	1.3

[a] Protein content of rat liver microsomes is 1280 mg/kg. Protein content of S9 fraction of dog liver, lung, and kidney is 3220, 425, and 423 mg/kg, respectively. f_b was 0.09.
[b] CL_{int} was calculated by $V_{max}/K_m \times$ (protein content).
[c] CL_{org} for liver and kidney was calculated by $Q \times f_b \times CL_{int}/(Q + f_b \times CL_{int})$, and that for lung was calculated by $f_b \times CL_{int}$.

Stereoselective Hydrolysis and Disposition of Butyryl-PL. The *R/S* ratios of the hydrolase activities in various tissues in rats and dogs are listed in Table 2. Butyryl-PL was (*R*)-preferentially hydrolyzed in dog plasma, liver, lung, and kidney. In rats, the enantiospecificity of the hydrolysis of butyryl-PL differed in various tissues. In particular, (*S*)-preferential hydrolysis and nonenantioselective hydrolysis were observed in the liver and in the plasma, respectively.

Table 4 shows the AUC of each enantiomer of PL and butyryl-PL after the intravenous administration of racemic PL or racemic butyryl-PL to rats (2.5 mg/kg, equivalent to PL) and dogs (2.0 mg/kg, equivalent to PL). In rats, the AUC_{plasma} of (*R*)-PL after the intravenous administration of racemic PL was greater than that of its antipode, in agreement with the findings of previous reports (Vermeulen et al., 1992). However, the AUC_{blood} of PL was equivalent for the two enantiomers after correction based on the blood/plasma ratio [Rb: *R*-PL, 0.55 ± 0.10; (*S*)-PL, 1.21 ± 0.25]. In addition, both the AUC_{plasma} and AUC_{blood} of (*R*)-butyryl-PL were 1.4-fold greater than those of the (*S*)-isomer after the intravenous administration of racemic butyryl-PL to rats. This may have been due to (*S*)-preferential hydrolysis of butyryl-PL in the rat liver. Moreover, the AUC_{blood} of converted (*R*)-PL after the administration of butyryl-PL was higher

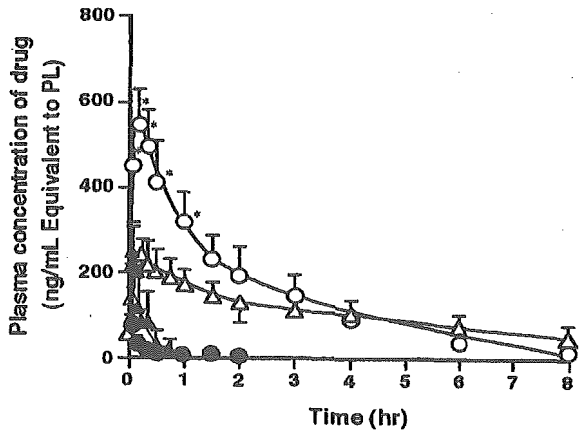

Fig. 4. Plasma concentrations of PL and butyryl-PL after intra-arterial and intravenous administration of butyryl-PL (2.0 mg/kg, equivalent to PL) in dogs. The circles and triangles indicate intravenous and intra-arterial administration, respectively. Open and closed symbols indicate the concentrations of converted PL and intact butyryl-PL, respectively. *, $p < 0.05$ compared with intra-arterial administration. Values are mean ± S.D. ($n = 4$).

TABLE 4

AUC (nanograms per hour per milliliter) and CL_{total} (liters per hour per kilogram) of each enantiomer after intravenous administration of racemic PL and butyryl-PL to rats (2.5 mg/kg, equivalent to PL) and dogs (2.0 mg/kg, equivalent to PL)

Administration[a]	Rat			Dog		
	R-Isomer	S-Isomer	R/S Ratio	R-Isomer	S-Isomer	R/S Ratio
PL						
$AUC_{plasma, PL}$	610	255	2.4	648 ± 231	672 ± 221	0.96 ± 0.08
$AUC_{blood, PL}$	336	309	1.1	517 ± 170	539 ± 177	0.96 ± 0.07
$CL_{total,PL}$	3.71	4.02	0.92	1.93 ± 0.61	1.85 ± 0.60	0.98 ± 0.09
Butyryl-PL						
$AUC_{plasma, Bu}$	281	199	1.4	7.51 ± 3.81	25.1 ± 3.89	0.30 ± 0.06
$AUC_{blood, Bu}$	250	180	1.4	6.12 ± 3.09	20.1 ± 3.11	0.30 ± 0.06
$AUC_{plasma, Bu\rightarrow PL}$	272	89.1	3.1	621 ± 185	634 ± 222	0.98 ± 0.05
$AUC_{blood, Bu\rightarrow PL}$	150	108	1.4	496 ± 147	508 ± 178	0.98 ± 0.06
$CL_{total,Bu}$	5.01	6.90	0.73	165 ± 84.4	49.8 ± 7.71	3.3 ± 1.1

[a] AUC of drugs after administration in rats was calculated from mean plasma concentrations from time zero to infinity. Rb values in the rat were (*R*)-PL, 0.55; (*S*)-PL, 1.2; (*R*)-butyryl-PL, 0.88; and (*S*)-butyryl-PL, 0.91. Rb values in the dog were (*R*)-PL, 0.80; (*S*)-PL, 0.80; (*R*)-butyryl-PL, 0.81; and (*S*)-butyryl-PL, 0.80. AUC_{blood} was calculated by AUC_{plasma} multiplied by Rb. CL_{total} was calculated from dose/AUC_{blood}.

than that of its antipode, possibly due to subsequent P450 metabolism of (*S*)-PL after (*S*)-preferential hydrolysis in the liver.

In dogs, the AUC_{plasma} and AUC_{blood} of PL after the intravenous administration of racemic PL were not significantly different for the two enantiomers. In addition, the AUC_{plasma} and AUC_{blood} of (*S*)-butyryl-PL were greater than those of (*R*)-butyryl-PL after the administration of racemic butyryl-PL in dogs, reflecting (*R*)-preferential hydrolysis in various tissues. However, the AUCs for the plasma and blood concentrations of PL converted from butyryl-PL were not enantioselective due to the nearly complete hydrolysis of both enantiomers within 10 min in various tissues, including the lung.

Inhibition of Hydrolysis of Butyryl-PL by BNPP. It has previously been demonstrated in inhibition experiments using several inhibitors for esterases that the hydrolysis of butyryl-PL in rat plasma and liver microsomes is catalyzed by carboxylesterase (Yoshigae et al., 1999). To identify the esterase involved in the hydrolysis of butyryl-PL in the dog liver and lung, BNPP was used as a selective inhibitor of carboxylesterase. The relative activity against various BNPP concentrations (10 nM–1 mM) is shown in Fig. 5. High concentrations of BNPP completely inhibited the hydrolysis of either enantiomer of butyryl-PL in microsomal fractions of the liver and lung, indicating that carboxylesterases are involved in the hydrolysis of butyryl-PL in these tissues. Moreover, BNPP inhibited the hydrolytic activity of cytosol in both tissues.

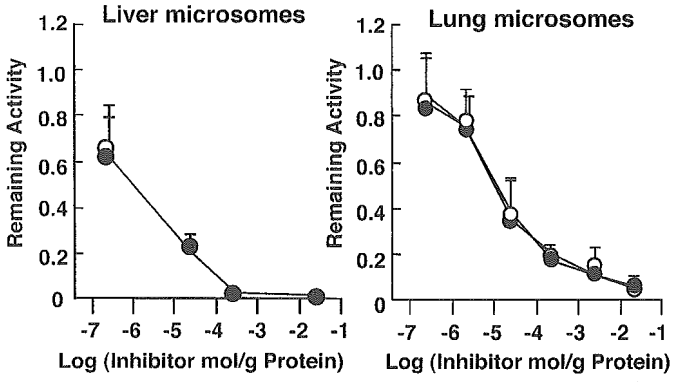

Fig. 5. Inhibition of the hydrolysis of each butyryl-PL enantiomer in dog liver and lung microsomes by BNPP. BNPP concentrations were 10 nM to 1 mM. Remaining activity values [○, (*R*)-isomer; ●, (*S*)-isomer] were plotted against the logarithm of mol of BNPP per gram of protein of microsomes. Values are mean ± S.D. (n = 3).

PAGE Electrophoresis of Subcellular Fraction of the Dog Liver and Lung. It is well known that the carboxylesterase activity present in microsomes is due to the binding of carboxylesterase to the ER (Satoh and Hosokawa. 1998). Despite the low hydrolase activity in the cytosol of any tissues in the rat, a relatively high cytosolic esterase activity was observed in the liver, lung, and kidney in the dog. To distinguish cytosol esterases from microsomal esterases, nondenaturing gel electrophoresis was performed. As shown in Fig. 6, nondenaturing gel electrophoresis of liver microsomes revealed two electrophoretically distinct esterases with activity toward 1-naphthylacetate. Dog liver cytosol also showed two bands at the same positions as for microsomes, indicating the presence of esterases similar to those in microsomes. The kidney also showed two bands, whereas the lung showed only the upper band in both the cytosol and microsomal fractions. These findings indicate that the dog liver and kidney express two types of esterase but the lung expresses only one. Furthermore, it is suggested that the cytosolic esterases are the same as the microsomal esterases in each tissue. Microsomal carboxylesterase that is loosely

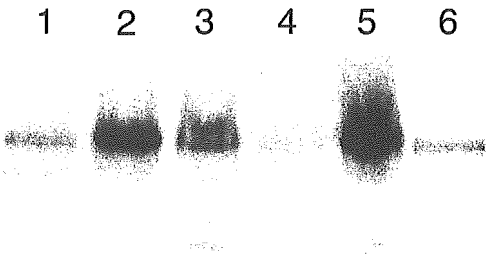

Fig. 6. Nondenaturing gel electrophoresis of dog tissue microsomes and cytosol. Staining for esterase activity was based on the formation of a red insoluble complex between Fast Red TR and 1-naphthol, which was released enzymatically from 1-naphthylacetate. Lanes 1 to 6 contained 35 μg of protein except lane 4 (130 μg of protein). Lane 1, lung cytosol; lane 2, lung microsomes; lane3, kidney microsomes; lane 4, kidney cytosol; lane 5, liver microsomes; and lane 6, liver cytosol.